16 (Fig. 5). Since DNA double strand breaks (DSBs)-containing chromosome domains are mobile [39], the DNA fragment of chromosome 16 might migrate to the breakage site of chromosome 17 where the *red/gam* reporter genes are present. Although further investigations are required to reveal the precise mechanisms by which DNA rearrangements are induced by MMC, the results strongly suggest that GDL1 cells are useful to investigate the molecular mechanisms of translocations induced by chromosome instability.

An intriguing feature of GDL1 cells is the higher spontaneous frequencies in the Spi$^-$ and *gpt* mutations compared to those of *gpt* delta mice (Tables 3 and 4). The spontaneous Spi$^-$ MFs in *gpt* delta mice are 1.1×10^{-6} in epidermis [12], 1.3×10^{-6} to 1.8×10^{-6} in bone marrow [7,8], 1.8×10^{-6} in spleen, 2.2×10^{-6} in liver, 2.4×10^{-6} in testis, and 2.6×10^{-6} in kidney [9]. Since spontaneous MF of Spi$^-$ selection in GDL1 cells was 25.6×10^{-6} (Table 3), it is 9.8–23-fold higher than the MFs in the organs of mice. Similarly, the spontaneous *gpt* MFs in *gpt* delta mice are 2.4×10^{-6} to 6.6×10^{-6} in liver [9,40], 6.0×10^{-6} in lung [41], 6.2×10^{-6} to 9.0×10^{-6} in colon [40,42], 8.2×10^{-6} in bone marrow [8], 12.1×10^{-6} in dermis, and 13.4×10^{-6} in epidermis [11]. The spontaneous MF of 6-TG selection in GDL1 cells was 22.7×10^{-6} (Table 4). The value is 1.7–9.5-fold higher than the MFs in various organs of *gpt* delta mice. In particular, the specific MF of class I mutations of Spi$^-$ (large deletions of a size more than 1 kbp) was more than 40 times higher in vitro (4.2×10^{-6}) than in vivo (0.1×10^{-6}) (Table 3). Even when we eliminated all possible clonally expanded class I mutants (Fig. 4), the specific MF was still about 20 times higher in GDL1 cells than in *gpt* delta mice. Single base deletions, i.e., class III mutants, also are more than 10 times higher in vitro (18.5×10^{-6}) than in vivo (1.5×10^{-6}). Most large deletions and single base deletions are probably due to the nonhomologous end-joining of DSBs in DNA and slippage errors during DNA replication, respectively. Thus, we suggest that spontaneous DNA strand breaks and slippage errors are more frequently induced in vitro than in vivo. Higher rates of cell proliferation in vitro compared with in vivo may be one reason for the higher incidence of DSBs and slippage errors in GDL1 cells.

Likewise, differences between in vitro and in vivo were seen in single base insertions and single base deletions in the spontaneous *gpt* mutations (Table 4). Eleven of forty-six (24%) mutations were single base insertions or small deletions in spontaneous *gpt* mutants in GDL1 cells (Table 2), and seven of them (7/11 = 64%) occurred in the DNA sequence in the run of the identical nucleotide (Fig. 6). On the contrary, in the *gpt* delta

mice, 4 of 29 mutations (14%) were single base deletions, and the mutations were not observed in the run of the identical nucleotide [8]. Not only in our cell lines but also in other cell lines having different lambda shuttle vectors for detection of mutations, insertions/deletions tend to be higher than those observed in the transgenic animals from which the cells originated [43–45]. Therefore, higher induction of deletion/insertion mutations is generally observed in cell lines carrying lambda shuttle vectors compared with in vivo. This tendency is expected to affect the increase in spontaneous MF more severely in Spi$^-$ selection than in 6-TG selection because Spi$^-$ selection is more sensitive to deletion/insertion mutations than 6-TG selection. In fact, the increase in spontaneous MFs was higher in Spi$^-$ selection (9.8–23-fold) than in 6-TG selection (1.7–9.5-fold) when compared between in vitro and in vivo as described above.

The combination of a lambda shuttle vector and a reporter gene is one of the most effective tools presently applicable for mutation analysis. Several cell lines have been established from TG mouse strains harboring the lambda vector system. Big Blue Rat2 [46], Big Blue mouse embryonic fibroblast cell lines [47], BBR/ME, BBR/OE, and BBR/MFib [48] are immortalized cell lines carrying *lacI* shuttle vectors. BBR1 and BBM1 are primary cultured cell lines from *lacI* transgenic mice [49]. EF1 is a cell line derived from *lacZ* transgenic mice [50]. However, the parent animals were insensitive to the MMC treatment or X-ray irradiation that effectively induces deletions [51,52]. Induction of large deletion mutations in these cells has not been reported. The sizes of the reporter genes are approximately 1 kbp in *lacI*, 3 kbp in *lacZ*, and 0.3 kbp in *cII* [2]. It may be difficult to detect large deletion mutations larger than the reporter genes. Additionally, highly predominant induction of base substitution mutations may hide an increase in deletion mutations because both the *lacI* and *lacZ* systems detect both point mutations and deletion mutations in a single selection system. Therefore, the result in the present study that GDL1 cells detected large deletion mutations suggests a distinct advantage.

It is common to use some agents that accelerate and/or accumulate mutations to establish a cell line from an animal tissue. A majority of the cell lines from the lambda vector TG rodent strains were established after treatment with strong mutagens for the purpose of immortalizing the cells. X-ray and benzo[*a*]pyrene were used for the Big Blue mouse embryonic fibroblast cell line [47]. *N*-Ethyl-*N*-nitrosourea was used for BBR/ME, BBR/OE, and BBR/MFib [48]. However, the SV40 T antigen gene was used to establish the GDL1 cells. This is the first attempt to apply the SV40 T antigen to the cell lines

for genotoxicity assays. Information on the biological functions of the SV40 T antigen may support better understanding of the responses of GDL1 cells to mutagens. The normal functions of p53 were lost in the CHL, CHO, and L5178Y tk$^{+/-}$ cells, which are commonly used in genotoxicity tests [53,54]. The dysfunction of p53 prevents the cells from apoptosis when the cells are damaged by mutagens. Since p53 plays an important role in DNA repair and genome stability, the dysfunction of the protein may increase the genetic damage by mutagens.

The present study demonstrates that the established GDL1 cell line detected large deletion mutations induced by MMC. The GDL1 cell is a useful tool for detecting various mutations including large deletion mutations, which covers all types of mutations induced in *gpt* delta mice. Although there are two differences in mutation spectra, i.e., single base substitution and complex rearrangement, between GDL1 cells and *gpt* delta mice after MMC treatment, the mutations detected in GDL1 cells are generally consistent with observations in *gpt* delta mice. A combination of GDL1 cell and gene targeting techniques, such as siRNA, knockout, or overexpression of target genes, may be an informative approach to understanding intracellular procedures involved in mutation and DNA repair.

Acknowledgement

References

[1] C.J. Shaw, J.R. Lupski, Implications of human genome architecture for rearrangement-based disorders: the genomic basis of disease, Hum. Mol. Genet. 13 (2004) 57–64.

[2] T. Nohmi, T. Suzuki, K. Masumura, Recent advances in the protocols of transgenic mouse mutation assays, Mutat. Res. 455 (2000) 191–215.

[3] J.A. Heddle, S. Dean, T. Nohmi, M. Boerrigter, D. Casciano, G.R. Douglas, B.W. Glickman, N.J. Gorelick, J.C. Mirsalis, H.J. Martus, T.R. Skopek, V. Thybaud, K.R. Tindall, N. Yajima, *In vivo* transgenic mutation assays, Environ. Mol. Mutagen. 35 (2000) 253–259.

[4] T. Nohmi, M. Katoh, H. Suzuki, M. Matsui, M. Yamada, M. Watanabe, M. Suzuki, N. Horiya, O. Ueda, T. Shibuya, H. Ikeda, T. Sofuni, A new transgenic mouse mutagenesis test system using Spi⁻ and 6-thioguanine selections, Environ. Mol. Mutagen. 28 (1996) 465–470.

[5] J.A. Gossen, H.J. Martus, J.Y. Wei, J. Vijg, Spontaneous and X-ray-induced deletion mutations in a *LacZ* plasmid-based transgenic mouse model, Mutat. Res. 331 (1995) 89–97.

[6] H. Louro, M.J. Silva, M.G. Boavida, Mutagenic activity of cisplatin in the *lacZ* plasmid-based transgenic mouse model, Environ. Mol. Mutagen. 40 (2002) 283–291.

[7] N. Okada, K. Masumura, T. Nohmi, N. Yajima, Efficient detection of deletions induced by a single treatment of mitomycin C in transgenic mouse *gpt* delta using the Spi⁻ selection, Environ. Mol. Mutagen. 34 (1999) 106–111.

[8] A. Takeiri, M. Mishima, K. Tanaka, A. Shioda, O. Ueda, H. Suzuki, M. Inoue, K. Masumura, T. Nohmi, Molecular characterization of mitomycin C-induced large deletions and tandem-base substitutions in the bone marrow of *gpt* delta transgenic mice, Chem. Res. Toxicol. 16 (2003) 171–179.

[9] K. Masumura, K. Kuniya, T. Kurobe, M. Fukuoka, F. Yatagai, T. Nohmi, Heavy-ion-induced mutations in the *gpt* delta transgenic mouse: comparison of mutation spectra induced by heavy-ion, X-ray, and gamma-ray radiation, Environ. Mol. Mutagen. 40 (2002) 207–215.

[10] T. Nohmi, M. Suzuki, K. Masumura, M. Yamada, K. Matsui, O. Ueda, H. Suzuki, M. Katoh, H. Ikeda, T. Sofuni, Spi⁻ selection: an efficient method to detect gamma-ray-induced deletions in transgenic mice, Environ. Mol. Mutagen. 34 (1999) 9–15.

[11] M. Horiguchi, K. Masumura, H. Ikehata, T. Ono, Y. Kanke, T. Sofuni, T. Nohmi, UVB-induced *gpt* mutations in the skin of *gpt* delta transgenic mice, Environ. Mol. Mutagen. 34 (1999) 72–79.

[12] M. Horiguchi, K.I. Masumura, H. Ikehata, T. Ono, Y. Kanke, T. Nohmi, Molecular nature of ultraviolet B light-induced deletions in the murine epidermis, Cancer Res. 61 (2001) 3913–3918.

[13] D.C. Doll, R.B. Weiss, B.F. Issell, Mitomycin: ten years after approval for marketing, J. Clin. Oncol. 3 (1985) 276–286.

[14] M. Tomasz, Y. Palom, The mitomycin bioreductive antitumor agents: cross-linking and alkylation of DNA as the molecular basis of their activity, Pharmacol. Ther. 76 (1997) 73–87.

[15] M. Tomasz, R. Lipman, D. Chowdary, J. Pawlak, G.L. Verdine, K. Nakanishi, Isolation and structure of a covalent cross-link adduct between mitomycin C and DNA, Science 235 (1987) 1204–1208.

[16] M. Tomasz, A.K. Chawla, R. Lipman, Mechanism of monofunctional and bifunctional alkylation of DNA by mitomycin C, Biochemistry 27 (1988) 3182–3187.

[17] K.G. Suresh, R. Lipman, J. Cummings, M. Tomasz, Mitomycin C-DNA adducts generated by DT-diaphorase. Revised mechanism of the enzymatic reductive activation of mitomycin C, Biochemistry 36 (1997) 14128–14136.

[18] Y. Palom, R. Lipman, S.M. Musser, M. Tomasz, A mitomycin-N^6-deoxyadenosine adduct isolated from DNA, Chem. Res. Toxicol. 11 (1998) 203–210.

[19] Y. Palom, M.F. Belcourt, S.M. Musser, A.C. Sartorelli, S. Rockwell, M. Tomasz, Structure of adduct X, the last unknown of the six major DNA adducts of mitomycin C formed in EMT6 mouse mammary tumor cells, Chem. Res. Toxicol. 13 (2000) 479–488.

[20] H. Ariga, S. Sugano, Initiation of simian virus 40 DNA replication in vitro, J. Virol. 48 (1983) 481–491.

[21] J.H. Bielas, J.A. Heddle, Proliferation is necessary for both repair and mutation in transgenic mouse cells, Proc. Natl. Acad. Sci. U.S.A. 97 (2000) 11391–11396.

[22] G.J. Carr, N.J. Gorelick, Mutational spectra in transgenic animal research: data analysis and study design based upon the mutant or mutation frequency, Environ. Mol. Mutagen. 28 (1996) 405–413.

[23] A.K. Basu, C.J. Hanrahan, S.A. Malia, S. Kumar, R. Bizanek, M. Tomasz, Effect of site-specifically located mitomycin C-DNA monoadducts on in vitro DNA synthesis by DNA polymerases, Biochemistry 32 (1993) 4708–4718.

[24] V.-S. Li, H. Kohn, Studies on the bonding specificity for mitomycin C-DNA monoalkylation processes, J. Am. Chem. Soc. 113 (1991) 275–283.

[25] N.S. Srikanth, A. Mudipalli, A.E. Maccubbin, H.L. Gurtoo, Mutations in a shuttle vector exposed to activated mitomycin C, Mol. Carcinog. 10 (1994) 23–29.

[26] A.E. Maccubbin, A. Mudipalli, S.S. Nadadur, N. Ersing, H.L. Gurtoo, Mutations induced in a shuttle vector plasmid exposed to monofunctionally activated mitomycin C, Environ. Mol. Mutagen. 29 (1997) 143–151.

[27] P.S. Jat, P.A. Sharp, Cell lines established by a temperature-sensitive simian virus 40 large-T-antigen gene are growth restricted at the nonpermissive temperature, Mol. Cell. Biol. 9 (1989) 1672–1681.

[28] J.M. Ruppert, B. Stillman, Analysis of a protein-binding domain of p53, Mol. Cell. Biol. 13 (1993) 3811–3820.

[29] R.S. Quartin, C.N. Cole, J.M. Pipas, A.J. Levine, The amino-terminal functions of the simian virus 40 large T antigen are required to overcome wild-type p53-mediated growth arrest of cells, J. Virol. 68 (1994) 1334–1341.

[30] S.M. Morris, A role for p53 in the frequency and mechanism of mutation, Mutat. Res. 511 (2002) 45–62.

[31] P.C. Hanawalt, Controlling the efficiency of excision repair, Mutat. Res. 485 (2001) 3–13.

[32] S. Adimoolam, J.M. Ford, p53 and regulation of DNA damage recognition during nucleotide excision repair, DNA Repair 2 (2003) 947–954.

[33] P.C. Hanawalt, J.M. Ford, D.R. Lloyd, Functional characterization of global genomic DNA repair and its implications for cancer, Mutat. Res. 544 (2003) 107–114.

[34] K.K. Bowman, D.M. Sicard, J.M. Ford, P.C. Hanawalt, Reduced global genomic repair of ultraviolet light-induced cyclobutane pyrimidine dimers in simian virus 40-transformed human cells, Mol. Carcinog. 29 (2000) 17–24.

[35] J.M. Ford, E.L. Baron, P.C. Hanawalt, Human fibroblasts expressing the human papillomavirus E6 gene are deficient in global genomic nucleotide excision repair and sensitive to ultraviolet irradiation, Cancer Res. 58 (1998) 599–603.

[36] F. Yatagai, T. Kurobe, T. Nohmi, K. Masumura, T. Tsukada, H. Yamaguchi, K. Kasai-Eguchi, N. Fukunishi, Heavy-ion-induced mutations in the gpt delta transgenic mouse: effect of p53 gene knockout, Environ. Mol. Mutagen. 40 (2002) 216–225.

[37] C. Zhu, K.D. Mills, D.O. Ferguson, C. Lee, J. Manis, J. Fleming, Y. Gao, C.C. Morton, F.W. Alt, Unrepaired DNA breaks in p53-deficient cells lead to oncogenic gene amplification subsequent to translocations, Cell 109 (2002) 811–821.

[38] M. Honma, M. Izumi, M. Sakuraba, S. Tadokoro, H. Sakamoto, W. Wang, F. Yatagai, M. Hayashi, Deletion, rearrangement, and gene conversion; genetic consequences of chromosomal double-strand breaks in human cells, Environ. Mol. Mutagen. 42 (2003) 288–298.

[39] J.A. Aten, J. Stap, P.M. Krawczyk, C.H. van Oven, R.A. Hoebe, J. Essers, R. Kanaar, Dynamics of DNA double-strand breaks revealed by clustering of damaged chromosome domains, Science 303 (2004) 92–95.

[40] K. Masumura, Y. Totsuka, K. Wakabayashi, T. Nohmi, Potent genotoxicity of aminophenylnorharman, formed from non-mutagenic norharman and aniline, in the liver of gpt delta transgenic mouse, Carcinogenesis 24 (2003) 1985–1993.

[41] A.H. Hashimoto, K. Amanuma, K. Hiyoshi, H. Takano, K. Masumura, T. Nohmi, Y. Aoki, In vivo mutagenesis induced by benzo[a]pyrene instilled into the lung of gpt delta transgenic mice, Environ. Mol. Mutagen. 45 (2005) 365–373.

[42] K. Masumura, M. Horiguchi, A. Nishikawa, T. Umemura, K. Kanki, Y. Kanke, T. Nohmi, Low dose genotoxicity of 2-amino-3,8-dimethylimidazo[4,5-f]quinoxaline (MeIQx) in gpt delta transgenic mice, Mutat. Res. 541 (2003) 91–102.

[43] C.N. Sprung, Y.P. Wang, D.L. Miller, D.D. Giannini, N. Dhananjaya, W.J. Bodell, Induction of lacI mutations in Big Blue Rat-2 cells treated with 1-(2-hydroxyethyl)-1-nitrosourea: a model system for the analysis of mutagenic potential of the hydroxyethyl adducts produced by 1,3-bis (2-chloroethyl)-1-nitrosourea, Mutat. Res. 484 (2001) 77–86.

[44] D.M. Zimmer, X.B. Zhang, P.R. Harbach, J.K. Mayo, C.S. Aaron, Spontaneous and ethylnitrosourea-induced mutation fixation and molecular spectra at the lacI transgene in the Big Blue rat-2 embryo cell line, Environ. Mol. Mutagen. 28 (1996) 325–333.

[45] J.C. Ryu, Y.J. Kim, Y.G. Chai, Mutation spectrum of 1,2-dibromo-3-chloropropane, an endocrine disruptor, in the lacI transgenic Big Blue Rat2 fibroblast cell line, Mutagenesis 17 (2002) 301–307.

[46] D.L. Wyborski, S. Malkhosyan, J. Moores, M. Perucho, J.M. Short, Development of a rat cell line containing stably integrated copies of a lambda/lacI shuttle vector, Mutat. Res. 334 (1995) 161–165.

[47] G.L. Erexson, M.L. Cunningham, K.R. Tindall, Cytogenetic characterization of the transgenic Big Blue Rat2 and Big Blue mouse embryonic fibroblast cell lines, Mutagenesis 13 (1998) 649–653.

[48] H.M. McDiarmid, G.R. Douglas, B.L. Coomber, P.D. Josephy, Epithelial and fibroblast cell lines cultured from the transgenic BigBlue rat: an in vitro mutagenesis assay, Mutat. Res. 497 (2001) 39–47.

[49] G.L. Erexson, D.E. Watson, K.R. Tindall, Characterization of new transgenic Big Blue® mouse and rat primary fibroblast cell strains for use in molecular toxicology studies, Environ. Mol. Mutagen. 34 (1999) 90–96.

[50] P.A. White, G.R. Douglas, J. Gingerich, C. Parfett, P. Shwed, V. Seligy, L. Soper, L. Berndt, J. Bayley, S. Wagner, K. Pound, D. Blakey, Development and characterization of a stable epithelial cell line from Muta Mouse lung, Environ. Mol. Mutagen. 42 (2003) 166–184.

[51] T. Suzuki, M. Hayashi, T. Sofuni, B.C. Myhr, The concomitant detection of gene mutation and micronucleus induction by mitomycin C in vivo using lacZ transgenic mice, Mutat. Res. 285 (1993) 219–224.

[52] K.S. Tao, C. Urlando, J.A. Heddle, Comparison of somatic mutation in a transgenic versus host locus, Proc. Natl. Acad. Sci. U.S.A. 90 (1993) 10681–10685.

[53] T. Hu, C.M. Miller, G.M. Ridder, M.J. Aardema, Characterization of p53 in Chinese hamster cell lines CHO-K1, CHO-WBL, and CHL: implications for genotoxicity testing, Mutat. Res. 426 (1999) 51–62.

[54] R.D. Storer, A.R. Kraynak, T.W. McKelvey, M.C. Elia, T.L. Goodrow, J.G. DeLuca, The mouse lymphoma L5178Y Tk$^{+/-}$ cell line is heterozygous for a codon 170 mutation in the p53 tumor suppressor gene, Mutat. Res. 373 (1997) 157–165.

Deletion and single nucleotide substitution at G:C in the kidney of *gpt* delta transgenic mice after ferric nitrilotriacetate treatment

Li Jiang,[1] Yi Zhong,[1] Shinya Akatsuka,[1] Yu-Ting Liu,[1] Khokon Kumar Dutta,[1] Wen-Hua Lee,[1] Janice Onuki,[1,2] Ken-ichi Masumura,[3] Takehiko Nohmi[3] and Shinya Toyokuni[1,4]

[1]Department of Pathology and Biology of Diseases, Graduate School of Medicine, Kyoto University, Kyoto 606-8501; [2]Laboratory of Biochemistry and Biophysics, Butantan Institute, São Paulo, SP, Brazil; [3]Division of Genetics and Mutagenesis, National Institute of Health Sciences, Tokyo 158-8501, Japan

An iron chelate, ferric nitrilotriacetate (Fe-NTA), induces oxidative renal proximal tubular damage that subsequently leads to a high incidence of renal cell carcinoma in rodents, presenting an intriguing model of free radical-induced carcinogenesis. In the present study, we used *gpt* delta transgenic mice, which allow efficient detection of point mutations and deletions *in vivo*, to evaluate the mutation spectra, in association with the formation of 8-oxoguanine and acrolein-modified adenine during the first 3 weeks of carcinogenesis. Immunohistochemical analysis revealed the highest levels of 8-oxoguanine and acrolein-modifed adenine in the renal proximal tubules after 1 week of repeated administration. DNA immunoprecipitation and quantitative polymerase chain reaction analysis showed that the relative abundance of 8-oxoguanine and acrolein-modified adenine at the *gpt* reporter gene were increased at the first week in the kidney. Similarly, in both 6-thioguanine and Spi⁻ selections performed on the renal specimens after Fe-NTA administration, the mutant frequencies were increased in the Fe-NTA-treated mice at the first week. Further analyzes of 79 mutant clones and 93 positive plaques showed a high frequency of G:C pairs as preferred targets for point mutation, notably G:C to C:G transversion-type mutation followed by deletion, and of large-size (>1 kilobase) deletions with short homologous sequences in proximity to repeated sequences at the junctions. The results demonstrate that the iron-based Fenton reaction is mutagenic *in vivo* in the renal tubular cells and induces characteristic mutations. (*Cancer Sci* 2006; 97: 1159–1167)

Oxidative stress is associated with a variety of pathological phenomena, including infection, inflammation, ultraviolet- and γ-irradiation, overload of transition metals and certain chemical agents.[1] Many epidemiological studies have demonstrated a close association between chronically oxidative conditions and carcinogenesis. For example, chronic tuberculous pleuritis causes a high incidence of malignant lymphoma;[2] asbestosis (asbestos fibers are rich in iron),[3] is often associated with mesothelioma and lung carcinoma;[4] chronic *Helicobacter pylori* infection is associated with a high incidence of gastric cancer;[5,6] the incidence of colorectal cancer is increased in ulcerative colitis;[7,8] a high risk for heptocellular carcinoma is observed in patients with genetic hemochromatosis, an iron overload disease;[9,10] severe burns by ultraviolet radiation is a risk factor for skin cancer;[11,12] and γ-irradiation causes a high incidence of leukemia.[13] At least under these circumstances, and probably in other types of carcinogenesis as well, oxidative stress appears to play a major role in human carcinogenesis.

An iron chelate, ferric nitrilotriacetate (Fe-NTA), causes oxidative renal proximal tubular injury via the Fenton reaction, and this injury ultimately leads to a high incidence of renal cell carcinoma in mice[14] and rats[15] after repeated intraperitoneal administration. This is an intriguing model in the following respects: (1) more than half of the induced tumors metastasize to the lung and/or invade the peritoneal cavity, resulting in animal mortality;[16] (2) convincing evidence exists regarding the involvement of free radical reactions in the carcinogenic process, including not only an increase in covalently modified macromolecules (oxidatively modified DNA bases[17] and lipid peroxidation products)[18,19] but also preventive effects of α-tocopherol fortification against carcinogenesis;[20] (3) genetic changes in the *p16^{INK4a}* tumor suppressor gene, especially homozygous deletions[21,22] and expressional alteration of several key genes, including annexin 2[23] and thioredoxin binding protein-2,[24] have been observed.

Fe-NTA itself is Ames test-negative,[14] but is positive in other cell culture systems detecting mutations.[25,26] Thus far, its mutation spectrum has not been comprehensively studied. Since the Ames test is a system involving prokaryotes, an assay system with the ability to detect mutations under *in vivo* conditions in which eukaryotic DNA repair mechanisms, metabolic pathways and other physiological systems are operative would offer significant advantages with respect to reliability. Based on this premise, several transgenic mouse mutagenesis assay systems have been developed, including Muta mice,[27] Big Blue mice[28] and HITEC mice.[29] These systems employ a recoverable transgenic lambda phage vector containing a reporter gene from bacteria. However, these systems all have the limitation that large deletions cannot be efficiently detected. We have developed a novel mutagenesis test system named *gpt* delta transgenic mice, which are transgenic for the *lambda EG 10* gene containing the *gpt* gene of *Escherichia coli*.[30] An important feature of this system is that both point mutations and large deletions can be tested concurrently in the targeted organs of the mice; point mutations are detected by 6-thioguanine (6-TG) selection and deletions larger than 1 kb can be identified by Spi⁻ (sensitive to P2 interference) selection. Thus far, various mutagens, including γ-ray irradiation, UVB, mitomycin C and PhIP, have been studied by using this *in vivo* system.[31]

In the present study, we used *gpt* transgenic mice to investigate the early genetic changes in Fe-NTA-induced renal carcinogenesis. Furthermore, we studied the relative abundance of two different types of DNA base modifications in several limited genomic loci with a novel technique called DNA immunoprecipitation (DnaIP), which selectively collects enzyme-digested DNA fragments

containing the target oxidative DNA base modification with specific monoclonal antibody. The present study for the first time revealed characteristics of the mutation spectrum in the kidney following repeated episodes of the Fenton reaction.

Materials and Methods

Animals and chemicals. *Gpt* delta C57BL/6 J transgenic mice were provided by Dr Takehiko Nohmi (Division of Genetics and Mutagenesis, National Institute of Health Sciences, Tokyo, Japan) and maintained in Kyoto University under specific-pathogen free and light-, temperature- and humidity-controlled conditions. The animal experiment committee of the Graduate School of Medicine, Kyoto University, approved the present experiments. $Fe(NO_3)_3 \cdot 9H_2O$ was obtained from Wako (Osaka, Japan). Nitrilotriacetic acid, disodium salt, was purchased from Nacalai Tesque (Kyoto, Japan). Fe-NTA was prepared immediately before use as described previously.[18] A total of 12 4-week-old male mice were used; nine mice were subjected to repetitive Fe-NTA administration and three mice were used as untreated controls. Mice were injected intraperitoneally with 3 mg iron/kg of Fe-NTA daily for three days, and the dose was increased to 5 mg iron/kg of Fe-NTA from the fourth day according to the established carcinogenesis protocol.[16] The injections were performed five times a week at approximately 10.00 hours. The animals were killed 48 h after the final administration. Both kidneys and the central lobe of the liver were immediately excised. Half of one kidney and a portion of the liver were used for histological and immunohistochemical analysis, and the rest of the kidney was frozen in liquid nitrogen and stored at $-80°C$ for mutational analyzes.

Monoclonal antibodies. Monoclonal antibody N45.1 recognizing 8-hydroxy-2′-deoxyguanosine (8-OHdG)[32] and monoclonal antibody mAb21 recognizing acrolein-2′-deoxyadenosine adduct (acrolein-dA)[33] were used.

Histological and immunohistochemical analyzes. Kidney specimens were fixed with phosphate-buffered 10% formalin and embedded in paraffin, cut at 3-μm thickness and stained with hematoxylin and eosin staining. For immunohistochemical analyzes, the avidin-biotin complex method with peroxidase was used as described previously.[32,33]

DNA immunoprecipitation and quantitative PCR analysis. To evaluate the relative abundance of Fe-NTA-induced oxidative DNA base modifications (8-OHdG and acrolein-dA) at desired genomic loci, we developed a technique designated as DnaIP (DNA immuno-precipitation).[34] More details will be published elsewhere.[35] Briefly, genomic DNA was extracted from each kidney of *gpt* delta transgenic mice with the NaI method (Wako) using argon gas-saturated buffer to avoid further oxidation during the extraction procedures.[36] Twenty μg of genomic DNA was digested with *Hae*III (TakaraBio, Shiga, Japan), and incubated with each antibody (10 μg of N45.1 or 2 μg of mAb21) in 10 mM phosphate-buffered saline, pH 7.4, containing 0.1% bovine serum albumin, for 3 h at 4°C in a 900-μL volume. The mixture was then incubated with 100 μL of Dynabeads M-280 sheep antimouse IgG (Dynal, Oslo, Norway) for another 3 h, washed sequentially with four different buffers (buffer 1: 0.1% sodium deoxycholate, 1% Triton X-100, 1 mM EDTA, 50 mM HEPES-KOH, 140 mM NaCl, pH 7.5; buffer 2: 0.1% sodium deoxycholate, 1% Triton X-100, 1 mM EDTA, 50 mM HEPES-KOH, 500 mM NaCl, pH 7.5; buffer 3: 0.1% sodium deoxycholate, 0.5% Nonidet P-40, 1 mM EDTA, 250 mM LiCl, 10 mM Tris-HCl, pH 8.0; and buffer 4: 1 × TE). Beads-bound DNA was recovered by incubating the beads with 80 μL of elution buffer (10 mM EDTA, 1% SDS, 50 mM Tris-HCl, pH 8.0) at 65°C for 10 min, and was amplified twice by PCR after ligation to an adaptor (sense, 5′-OH-GGAATTCGGCGGCCGCGCGGATCC-3′; antisense, 5′-GGATCC-GCGGCCGCCG-3′; sense oligonucleotides were used as primers for amplification), treated with exonuclease I (TakaraBio) and

purified with phenol-chloroform extraction. The purified products were subjected to Real-Time PCR (7300 Real Time PCR System, Applied Biosystems, Tokyo) using Platinum SYBR Green qPCR SuperMix UDG (Invitrogen, Tokyo). The primer pairs used were as follows: *gpt*, forward-5′-GCCTTCTGAACAATGGAAAGG-3′, reverse-5′-CGTGATCGTAGCTGGAAATAC-3′ (125 bp); β-*actin*, forward-5′-TCCAACAAACCAAGAGAAATCC-3′, reverse-5′-CGACCTCTGAAACAATTCTGGT-3′ (108 bp); C15-49–5 (chromosome 15, extrageneic region), forward-5′-TGGTACCTGAGT-AAGGCAAGGT-3′, reverse-5′-CCCACTTGTGATTGCTTTCTTC-3′ (107 bp); C16-47–2 (chromosome 16, extrageneic region): forward-5′-CACACACACATGCACACTGTACT-3′, reverse-5′-GCATTTCTCCTCACATTCAGACT-3′ (114 bp); C16-47–5 (chromosome 16, extrageneic region): forward-5′-CCAATTGG-AGCTAACAGAAACC-3′, reverse-5-AGCTGGTCAACTGCC-TACTCTC-3′ (125 bp). These three extrageneic areas were selected based on our observations that chromosome 15 is peripherally located and chromosome 16 is centrally located in the murine renal tubular cells at interphase.[35]

In vitro phage packaging. Genomic DNAs were extracted with the phenol-chloroform extraction protocol.[37] Trangenic *lambda EG10* DNA was rescued from the host genomic DNA using Transpack Packaging Extract (Stratagene, La Jolla, CA) according to the manufacturer's instructions.[30]

Mutation analysis. The 6-TG mutation assay protocol has been described elsewhere.[38–40] Briefly, rescued phage was infected into YG 6020 *E. coli* expressing Cre enzyme, converted into a plasmid carrying the *Cm-resistance* gene and *gpt* gene, and poured on plates containing chloramphenicol (Cm) with or without 6-TG. The positive clones carrying the mutant *gpt* gene were obtained from 6-TG selection plates by incubating at 37°C for 96 h. Selected clones were confirmed again by plating on 6-TG selection plates. The whole *gpt* sequence was amplified from positive clones and identified by sequencing with an ABI PRIZM 377 sequencer. The primers used for amplifying and sequencing were as follows: forward-5′-GCGCAACCTATTTTCCCCTCGA-3′ and reverse-5′-TGGAAACTATTGTAACCCGCCTG-3′. The same primer pair was used for direct sequencing.[41] *E. coli* XL1-Blue MRA and XL1-Blue MRA (P2) were infected with the packaged phage. *E. coli* XL1-Blue MRA was poured onto NZY plates and XL1-Blue MRA (P2) was poured onto I-trypticase agar plates. Plaques that grew on the XL1-Blue MRA (P2) plates were selected and further confirmed with *E. coli* XL1-Blue MRA, *E. coli* WL95 (P2) and XL1-Blue MRA (P2). Positive plaques were recovered and used for determining the deletion position of the *red/gam* gene. Clones or plaques were counted for determining mutant frequencies (MFs). MFs were calculated by using established methods as described previously.[30,42,43]

Hybridization assay and PCR analysis for Spi⁻ mutant analysis. A protocol for Southern blot analysis for Spi⁻ (sensitive to P2 interference) mutants has been established.[43] Seventeen oligomers located within ~14 kb flanking sequence of the *red/gam* gene were used as probes for identifying the deletion junctions. These oligomers were named 18874R, 19258R, 20341R, 21328R, 22556R, 22869R, 23921R, 24858R, 25389F, 26704F, 27096F, 28165F, 29290F, 30104F, 31070F, 31879F and 32890F according to their position as described.[43] The oligomers were spotted onto Hybond™-N⁺ membrane (Amersham) and cross-linked with UV. PCR products, which were amplified by primer 18874R and 32890F using positive individual plaques as templates, were labeled with $(\alpha\text{-}^{32}P)$ dCTP using the Megaprime DNA labeling System (Amersham). The membranes were incubated with labeled PCR products at 50°C overnight, washed three times and exposed to BioMax film (Kodak, New York, NY). Deleted regions were located within those oligomers whose signals could not be observed on the film. The nearest primers were selected for PCR amplification and the PCR products were subjected to sequencing to determine the exact deletion junction.

Fig. 1. Immunohistochemical analysis of 8-hydroxy-2′-deoxyguanosine (8-OHdG) and acrolein-modified 2′-deoxyadenosine after repeated administration of ferric nitrilotriacetate (Fe-NTA). (a–d) Hematoxylin and eosin (HE) staining. Regenerative proximal tubular cells were prominent at the first week, together with some necrotic cells (b, ►). At the second and third week, necrotic cells were no longer observed but increasing numbers of karyomegalic cells (c and d, ♪) appeared. (e–h) Immunohistochemistry of 8-OHdG. Nuclear immunopositivity was observed after Fe-NTA administration, with the highest level after repeated administration for 1 week (f). (i–l) Immunohistochemistry of acrolein-dA. Nuclear immunopositivity was observed after Fe-NTA administration with that of repeated administration of 1 week the highest level (j). Refer to the Materials and Methods section for details (bar in l, 50 μm).
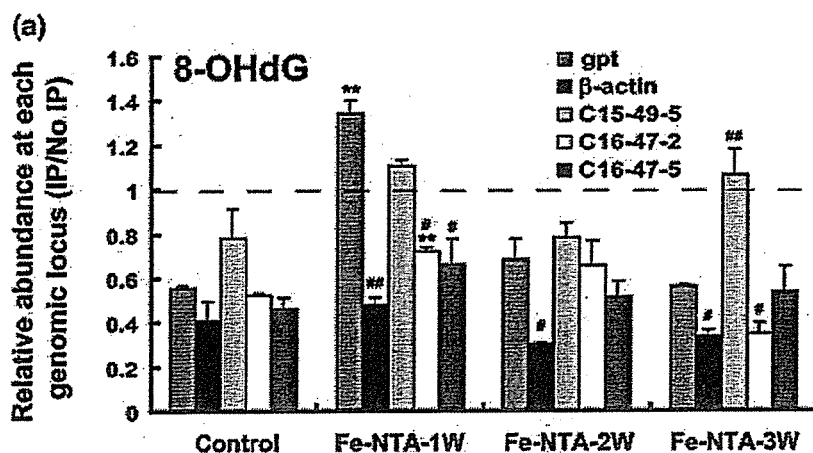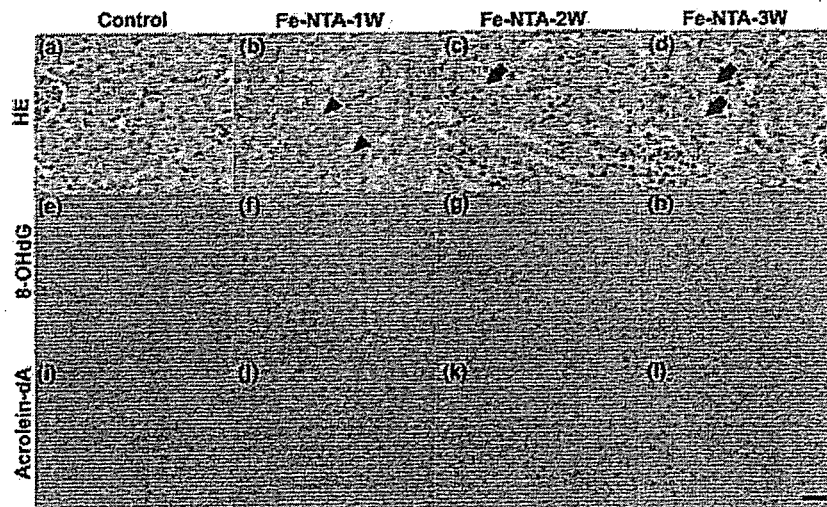
Fig. 2. Real-time polymerase chain reaction (RT-PCR) analysis after DNA immunoprecipitation for quantitation of oxidatively modified DNA bases at specific genomic loci. Renal genomic DNA was digested with HaeIII and subjected to immunoprecipitation (IP) with specific monoclonal antibodies against 8-hydroxy-2′-deoxyguanosine (8-OHdG) and acrolein-dA. The recovered DNA fragments were amplified after ligation to an adapter and were used as substrates for RT-PCR analyses of gpt, β-actin and three extrageneic regions at chromosome 15 or 16. Data are shown as relative abundance of PCR products amplified from recovered genomic DNA by IP per those amplified from the original genomic DNA in the same amounts. (a) 8-OHdG. (b) Acrolein-dA. Refer to the Materials and Methods section for details ($N = 3$, means ± SEM; $*P < 0.05$, $**P < 0.01$ versus untreated control kidney at the same genomic region; $\#P < 0.05$, $\#\#P < 0.01$ versus gpt locus data of the same treatment group).
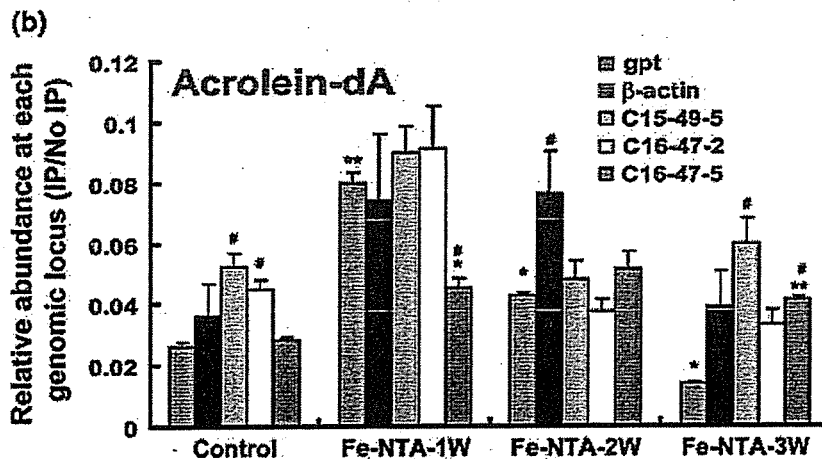
Statistical analysis. Statistical analyzes were performed with an unpaired t-test, which was modified for unequal variances when necessary.

Results

Renal histology after repeated Fe-NTA administration. As shown in Fig. 1a, no significant histological changes were observed in the kidney of the untreated control group. In contrast, pyknotic nuclei of proximal tubular cells revealing degeneration were scattered in the kidney of mice after 1 week of Fe-NTA treatment (Fig. 1b). Degenerative tubular cells were no longer observed there after 2 or 3 weeks of repeated Fe-NTA treatment, but atypical regenerative cells with a large nucleus containing prominent nucleoli were gradually increased (Fig. 1c,d). In either case, histological evaluation of the liver showed no apparent alterations (data not shown).

Jiang et al.

Oxidative DNA damage induced by repeated Fe-NTA administration.
Two major oxidative DNA base modifications, 8-OHdG and
acrolein-dA, were evaluated with immunohistochemistry and
DnaIP. Intense diffuse nuclear immunostaining of 8-OHdG
and acrolein-dA was prominent in the renal proximal tubules
after repeated Fe-NTA administration for 1 week, and gradually
decreased thereafter (Fig. 1e–l). To assess whether these oxidative
modifications were increased in the *gpt* gene locus, quantitative
PCR analysis after DnaIP was performed. The *gpt* reporter gene
locus after 1 week of repeated Fe-NTA administration showed
higher amounts of 8-OHdG and acrolein-dA than that in the
untreated control group. Similar patterns were also observed in
the other loci examined, but the *gpt* locus was the most sensitive
at the first week (Fig. 2), consistently with the immunohistoch-
emical data (Fig. 1e–l).

Fe-NTA-induced mutant frequencies in *gpt* and *red/gam* genes.
We then investigated the reporter genes, *gpt* and *red/gam*, to analyze
Fe-NTA-induced mutations using the 6-TG and Spi⁻ selection
systems. In both 6-TG and Spi⁻ selections, the mutation frequencies
were significantly increased (2.44-fold increase in 6-TG selection
and 1.72-fold increase in Spi⁻ selection) after 1 week of repeated
Fe-NTA administration (Fig. 3), which was consistent with the
results of immunohistochemistry (Fig. 1e–l) and DnaIP (Fig. 2).

Fe-NTA-induced *gpt* gene mutations. To further characterize the
exact *gpt* mutations caused by Fe-NTA, 79 mutant clones, in
which 69 clones were from Fe-NTA-treated mice and 10 from
untreated control mice, were analyzed (Table 1 and Fig. 4).
Among the mutations induced by Fe-NTA, 75.4% (52/69)
were single base substitutions, of which more than half (32/
52 = 61.5%) occurred at G:C base pairs, whereas GC content of
gpt gene was 46.6%. Among the Fe-NTA-induced substitutions,
40.4% (21/52) were transitions, including G:C to A:T (13/21)
and A:T to G:C (8/21), whereas the rest of substitutions (31/
52 = 59.6%) were transversions, including G:C to T:A (5/31),
G:C to C:G (14/31), A:T to T:A (4/31) and A:T to C:G (8/31)
(Table 1). In addition, 17.4% (12/69) of mutant clones were
identified as carrying single- or mutiple-base deletions. Among
them, 9/12 were single-base deletions, which occurred preferentially
at repeated sequences (Table 1 and Fig. 4). Four insertional
mutations and one tandem base substitution were also observed.
In contrast, analyses of a total of 10 clones from the untreated
control kidney showed that 8/10 were single-base substitutions
with a single-base deletion and an insertion. In either case,
complex mutations were not observed. Therefore, the results
indicated that Fe-NTA-induced *gpt* gene mutation preferentially
consisted of single-base substitutions occurring at G:C base
pairs, in which transversions were more frequent than transitions
(Table 1).

Fe-NTA-induced Spi⁻ mutations. To characterize the Spi⁻ muta-
tions induced by Fe-NTA, 93 positive plaques obtained from either
the kidneys of Fe-NTA-treated mice or untreated control mice
were screened by Southern blot analysis followed by sequencing
that resulted in the confirmation of 21 large-size deletions (Fig. 5a).
Large-size deletions were at first roughly positioned on ~14
kb of sequence spanning the *red/gam* gene by the use of 17
different oligomers as probes. We detected signals for all the 17
oligomer probes in the blot with hybridization to the wild-type
lambda EG 10 (Fig. 5b i). Signals for certain oligomers were
absent with Spi⁻ mutant plaques containing large-size deletions,
as shown in Fig. 5(b ii–iv). Most of the large deletions induced
by Fe-NTA were more than 1 kb in size (Class I mutation,[31])
(Fig. 5a). Furthermore, the majority of them (70.6%) had short
homologous sequences of 1–6 bp at the junctions (Class I-A),
and in many cases showed three bp or longer running sequences
at the junction or its vicinity. Five cases of large-size deletions
were accompanied by simultaneous single-base deletion in the
red/gam gene (Fig. 5a).

Discussion

In the present experiments we have for the first time studied the
mutation spectrum of the Fenton reaction-based renal tubular
damage in a model of oxidative stress-induced carcinogenesis
mediated by Fe-NTA. We intentionally avoided the acute
periods for evaluation because of the abundance of necrosis
and apoptosis,[20,44] and thus used the subacute phase when the
majority of the tubular cells become resistant to oxidative stress
with rare cell death present (Fig. 1b–d), though mutation spectrum
might be slightly different between the acute and subacute phases.
The accumulation of two different kinds of oxidative DNA base
modifications, 8-OHdG and acrolein-dA, was most evident
with immunohistochemistry after the first week of repeated
administration of Fe-NTA and gradually decreased thereafter
(Fig. 1e–l). This is probably due to the activation in the cellular
metabolic pathways for those either suppressing the Fenton
reaction or promoting DNA repair mechanisms. It is also possible
that cellular selective processes worked to remove heavily damaged
cells.

Gpt delta transgenic mice are an established model for analyzing
mutations *in vivo*, and have been used to analyze several possible
mutagens.[31] Here we have used a technique designated as
DnaIP to evaluate the relative abundance of the two DNA base
modifications at the *gpt* loci. Approximately 80 copies of the

(a)

(b)
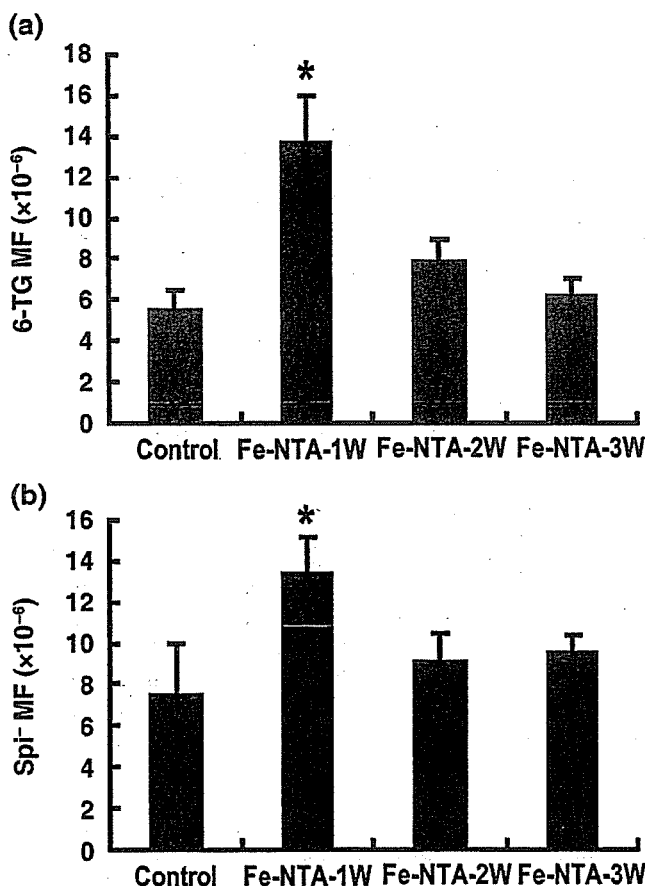
Fig. 3. Mutant frequency (MF) of 6-TG and Spi⁻ seletion. 6-TG selection
was used for the detection of base substitutions in the *gpt* gene;
Spi⁻ selection was used for the detection of large-size deletions. Refer
to the Materials and Methods section for details. (*N* = 3, means ± SEM;
*P < 0.05, **P < 0.01 *versus* untreated control kidney).

Table 1. Spectrum of Fe-NTA-induced mutations in the kidney of *gpt* delta transgenic mice

Mutation type	Nucleotide position	Sequence change	Amino acid change	Fe-NTA			Control
				1w	2w	3w	
Transition					30.4%		50.0%
G:C–A:T	27	G–A	Trp–STOP	1			
	39	G–A	Gln–Gln				1
	64	C–T	Arg–STOP	1			1
	110	G–A	Arg–His	5			1
	113	G–A	Arg–His				1
	116	G–A	Arg–Arg			1	
	128	G–A	Val–Met		1	1	
	287	C–T	Thr–Ile	1			
	356	G–A	Arg–His		1		
	447	C–T	Ile–Ile			1	
A:T–G:C	2	T–C	Met–Thr		1		
	25	T–C	Trp–Ser	1	2		
	188	A–G	Tyr–Cys		1		
	275	A–G	Asp–Gly				1
	307	A–G	Met–Val	1			
	410	A–G	Gln–Arg		1		
	415	T–C	Trp–Arg			1	
Transversion					44.9%		30.0%
G:C–T:A	3	G–T	Ser–Ile		1		
	110	G–T	Arg–His		1		
	115	G–T	Gly–Cys	1			
	189	C–A	Tyr–STOP	1			
	324	C–A	His–Gln				1
	418	G–T	Asp–Try	1			
G:C–C:G	109	C–G	Arg–Gly			1	
	125	C–G	Pro–Arg			1	
	238	G–C	Asp–His			1	
	297	G–C	Ala–Ala	2			
	413	C–G	Pro–Arg	2	1		
	414	G–C	Pro–Pro	2			
	427	G–C	Val–Leu	1		1	
	430	G–C	Val–Leu	2			1
A:T–T:A	52	A–T	Lys–STOP	1			
	66	A–T	Arg–Arg			1	
	179	T–A	Ile–Asn		1	1	
A:T–C:G	94	A–C	Ile–Leu		1		
	133	T–G	Phe–Val		1		
	134	T–G	Gly–STOP		1	1	
	146	A–C	Glu–Ala		1		
	286	A–C	Thr–Pro	1		1	
	315	A–C	Pro–Pro	1			
	375	T–G	Tyr–STOP				1
Deletions					17.4%		10.0%
1 base pair	8–12	AAAAA–AAAA		1	3	1	1
	88–90	AAAGG–AAGG				1	
	423–425	GGGCG–GGCG		1			
	430	TCGTA–TCTA				1	
	437	CGTCC–CGCC				1	
>2 base pairs	156–162	ATTCGTCATGT–ATCG			1		
	170–171	TACCG–TAG			1		
	252–253	TTCATC–TTTC			1		
Insertions					5.7%		10.0%
	74–75	CCTT–CCAATT				1	
	122–123	GTAC–GTTAC		1			
	310–311	ATCC–ATTCC			1	1	
	440–441	CCGC–CCCGC					1
Other					1.4%		0.0%
CC–AG	124–125	TACCGG–TAAGGG			1		

```
     atgagcgaaaaatacatcgtcacctgggacatgttgcagatccatgcacgtaaactcgca
c                    x                            a
1W                   x            c a                        t
2W   ct              x(3)         c(2)
3W                   x
     agccgactgatgccttctgaacaatggaaaggcattattgccgta agccgtgg ggtctg
c        t                                              a  a
1W       t                                              a(5)   t
2W                                          c           t
3W       t      â                  x                    g       a
     gtaccgggtgcgttactggcgcgtgaactgggtattcgtcatgtcgataccgtttgtatt
c
1W   t
2W   ag  a    gg           c        xxxxxx      xx      a
3W       g  a    g                                      a
     tccagctacgatcacgacaaccagcgcgagcttaaagtgctgaaacgcgcagaaggcgat
c
1W        a
2W        g
3W                                                              c
     ggcgaaggcttcatcgttattgatgacctggtggataccggtggtactgcggttgcgatt
c                        g
1W                                        ct          c(2)
2W           xx
3W                                        c
     cgtgaaatgtatccaaaagcgcactttgtcaccatcttcgcaaaaccggctggtcgtccg
c                        a
1W       g    c
2W           t                                         a
3W           t
     ctggttgatgactatgttgttgatatcccgcaagatacctggattgaac agccgtgg at
c            g
1W                                                  (2)gc(2)  t
2W                                             g   g
3W                                                  c
     atgggcgtcgtattcgtcccgccaatctccggtcgctaa
c            c              â
1W   x  c    c(2)
2W
3W      c  x       x        t
```

Fig. 4. The position of point mutations in the *gpt* gene. Refer to the Materials and Methods section for details (x, deletion; ^, insertion; underline, more than one base pair deletion within the same case; the number in parenthesis indicates the multiplicity of the same mutation. Square (in one letter), mutation-prone area with the same sequence.

transgenes are included per haploid genome in the *gpt* delta transgenic mice.[30] Among genomic loci examined, including β-actin and three extrageneic regions, the *gpt* loci showed the highest level of 8-OHdG and acrolein-dA after one week of repeated Fe-NTA administration (Fig. 2). This consistency with the immunohistochemical data demonstrates that the transgenic *gpt* loci are indeed vulnerable and suitable for mutational analyzes. We believe that the high copy number of the *gpt* gene contained in these mice is at least partially responsible for this reliable sensitivity. In contrast to the findings at one week, certain extrageneic loci showed significantly higher levels of DNA base modifications than the *gpt* gene locus at other time points, suggesting that further studies would be necessary to elucidate the principles governing the distribution of oxidative DNA base modifications over the whole genome.[35,45]

Mutation frequencies both for the 6-TG selection and Spi⁻ selection also were the highest at the first week of repeated Fe-NTA administration (Fig. 3). This confirms the usefulness of 8-OHdG and acrolein-dA, which were detected both by immunohistochemistry and DnaIP, as reliable markers of mutation. In 22.7% of the Spi⁻ plaques after Fe-NTA treatment, large-size deletions (>1 kb) were observed and most of them were class I-A mutants (Fig. 5). This preference for large-size deletions with short homologous sequences at the junctions might be a prominent feature of the results obtained in this renal carcinogenesis model in that the patterns of Spi⁻ mutations are similar to that of the untreated colon.[31] With γ-rays, shorter deletions than 1 kb are prominent; with UVB and

MMC, large-size deletions with or without short homologous sequences at the junctions are more frequently observed (>40%); whereas with PhIP and APNH, large-size deletions were rare.[31]

In the Fe-NTA-induced renal cell carcinoma of rats, homozygous deletion of the $p16^{INK4A}$ tumor suppressor gene was frequently observed,[21] and the allelic loss of this locus was observed at a high frequency one to three weeks after the repeated administration of Fe-NTA in rats.[22] We believe that the iron-mediated Fenton reaction is mainly responsible for this characteristic deletion. Short deletions were also increased after Fe-NTA administration (Table 1). Probably, the free radical reaction associated with iron is distinct from the reactions associated with other agents studied so far in the *gpt* lambda transgenic mice in that this is a universal reaction, though exaggerated through iron overload, involving the generation of hydroxyl radical and lipid peroxidation products. This kind of reaction is always taking place in the body under conditions of normal metabolism associated with oxygen consumption and, though it results in only minor consequences under physiological conditions, can be a driving force of carcinogenesis.

The mutation spectrum detected in the *gpt* gene was also quite distinctive. G:C pairs were the preferred bases for mutation, and especially G:C to C:G transversion-type mutation was characteristic (Fig. 4 and Table 1). This type of mutation was observed in PhIP and MMC as a minor type, but has not been reported as a major type of mutation (Table 2). We observed a low incidence of G:C to T:A transversion-type mutation that results from
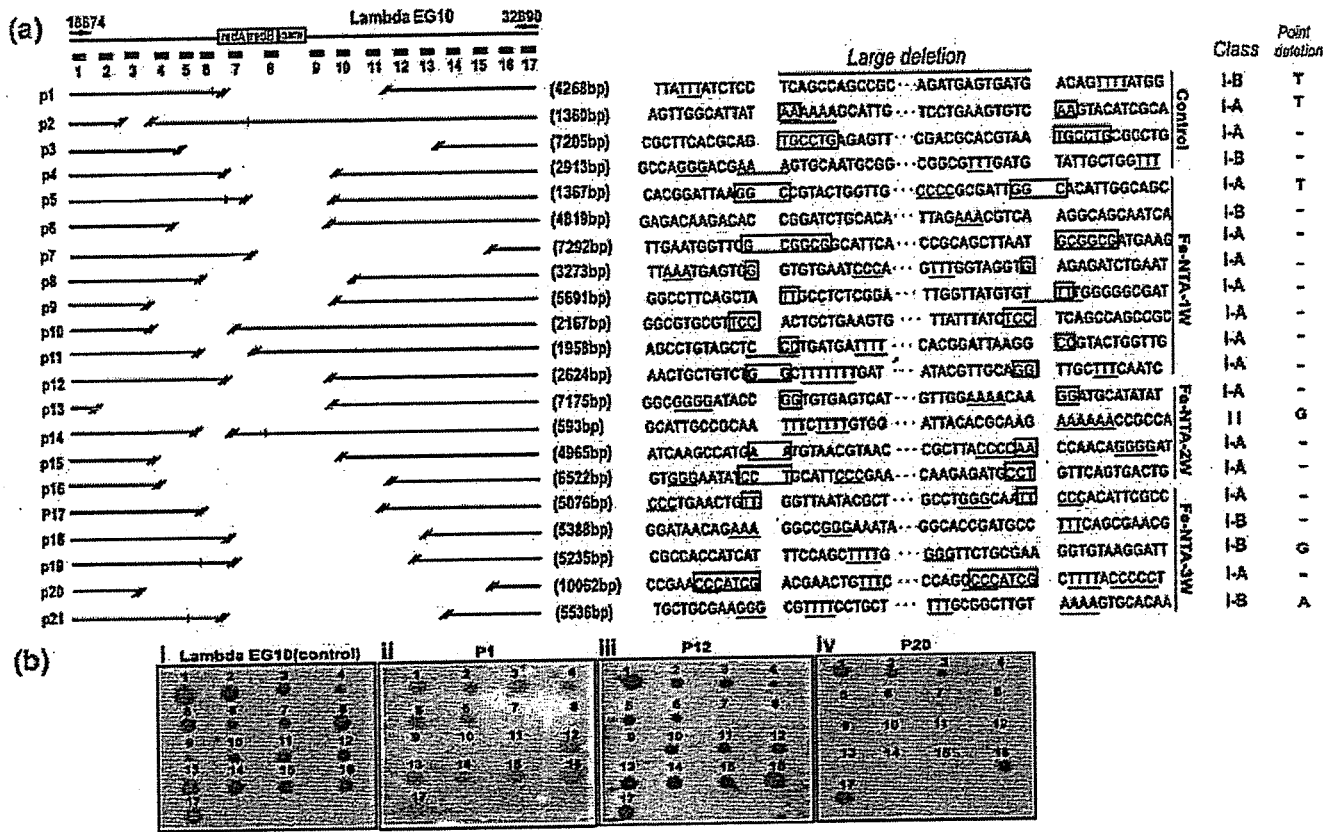
(a)

		Large deletion		Class	Point deletion
p1	(4268bp)	TTATTATCTCC TCAGCCAGCCGC···AGATGAGTGATG ACAGTTTATGG		I-B	T
p2	(1368bp)	AGTTGGCATTAT AAAAAAGCATTG···TCCTGAAGTGTC GAGTACATCGCA		I-A	T
p3	(7205bp)	CGCTTCACGCAG TTGCCTGAGAGTT···CGACGCACGTAA TTGCCTGCGCCTG		I-A	−
p4	(2913bp)	GCCAGGGACGAA AGTGCAATGCGG···CGGCGTTTGATG TATTGCTGGTTT		I-B	−
p5	(1367bp)	CACGGATTAAGG CCGTACTGGTTG···CCCCGCGATTGG CACATTGGCAGC		I-A	T
p6	(4819bp)	GAGACAAGACAC CGGATCTGCACA···TTAGAAACGTCA AGGCAGCAATCA		I-B	−
p7	(7292bp)	TTGAATGGTTCG CGGCGGCATTCA···CCGCAGCTTAAT GCGGCGATGAAG		I-A	−
p8	(3273bp)	TTAAATGAGTCG GTGTGAATCCCA···GTTTGGTAGGTG AGAGATCTGAAT		I-A	−
p9	(5691bp)	GGCCTTCAGCTA TTGCCTCTCGGA···TTGGTTATGTGT TTTGGGGGCGAT		I-A	−
p10	(2167bp)	GGCGTGCGTTCG ACTGCTGAAGTG···TTATTTATCTCG TCAGCCAGCCGC		I-A	−
p11	(1958bp)	AGCCTGTAGCTC GGTGATGATTTT···CACGGATTAAGG GGTACTGGTTG		I-A	−
p12	(2624bp)	AACTGCTGTCTG GCTTTTTTTGAT···ATACGTTGCAGG TTGCTTTCAATC		I-A	−
p13	(7175bp)	GGCGGGGATACC GGTGTGAGTCAT···GTTGGAAAACAA GGATGCATATAT		I-A	−
p14	(593bp)	GCATTGCCGCAA TTTCTTTTGTGG···ATTACACGCAAG AAAAAACCGCCA		II	G
p15	(4965bp)	ATCAAGCCATCA ATGTAACGTAAC···CGCTTACCCCAA CCAACAGGGGAT		I-A	−
p16	(6522bp)	GTGGGAATATCC TGCATTCCCGAA···CAAGAGATGCCT GTTCAGTGACTG		I-A	−
p17	(5076bp)	CCCTGAACTGTT GGTTAATACGCT···GCCTGGGCAATT CCCACATTCGCC		I-A	−
p18	(5388bp)	GGATAACAGAAA GGCCGGGAAATA···GGCACCGATGCC TTTCAGCGAACG		I-B	−
p19	(5235bp)	CGCCACCATCAT TTCCAGCTTTTG···GGGTTCTGCGAA GGTGTAAGGATT		I-B	G
p20	(10052bp)	CCGAACCCATCG ACGAACTGTTTC···CCAGCCCCATCG CTTTTACCCCCT		I-A	−
p21	(5536bp)	TGCTGCGAAGGG CGTTTTCCTGCT···TTGCGGCTTGT AAAAGTGCACAA		I-B	A

(b)

Fig. 5. Size and position of large-size deletions after Spi⁻ selection with each junctional sequence. (a) Summary of the strategy and the observed deletions. P1–P4, untreated control; P5–P21, ferric nitrilotriacetate (Fe-NTA)-induced deletions. Blank areas between two double-dash lines indicate large-size deletions; short longitudinal lines indicate accompanying 1-base deletion; □, short homologous sequence; underline, short run more than 3 bp. Classification of the deletion type was done as described.[31] (b) Representative results of Southern blotting analysis for screening the deleted positions. Arabic numerals (1–17) indicate the probes used as described in the Materials and Methods section and P1, P12 and P20 correspond to the a section.

8-OHdG formation.[46,47] This may be explained by the fact that this mutagenic process is strongly inhibited by a DNA repair enzyme, Mutyh.[48] Here we may propose a mechanism in which certain oxidative modification to guanine/cytosine may cause abnormal pairing with the same corresponding base. Recently, it was reported that formamidopyrimidine (FaPy)-guanine, another oxidative DNA base modification,[49,50] would not be responsible for this type of mutation.[51] We suspect that 5,6-dihydroxyuracil and 5-hydroxycytosine which are increased in this model[17] or other aldehyde-modified bases than acrolein-dA are among the possible candidates.

When we reviewed the spectrum of point mutation observed in the *p53, tsc2, p15, p16 and tbp-2* tumor suppressor genes of Fe-NTA-induced rat renal carcinoma, we observed no G:C to C:G transversions, but G:C to T:A (*p53, tbp-2*),[16,24] T:A to C:G (*tsc2*), G:C to A:T (*p15 and p16, tbp-2*),[21] A:T to T:A (*tbp-2*)[24] and one nucleotide insertion/deletion at repeat sequences (*p16, tbp-2*)[21,24] were observed despite the limited available data. There are at least several possibilities to explain this: (i) we have not yet identified the target genes with G:C to C:G mutations; (ii) there are some species-differences between mice and rats; (iii) this mutation spectrum detected in this *gpt* transgenic system is largely reflected in non-geneic genome areas; and (iv) the last possibilities are that G:C to C:G mutations are preferentially repaired by mismatch repair enzyme(s) in non-transgene areas or abundant mutations of this kind lead to

lethal effects, affecting fundamental transcriptional activity in the expressed genes. Regarding species differences, another study using the *gpt* delta transgenic rat[52] would answer the question. The data obtained with DnaIP is of note in that 8-OHdG and acrolein-dA were increased in some non-geneic regions after three weeks of repeated administration of Fe-NTA, warranting further studies.

In conclusion, we used the *gpt* delta transgenic mice to evaluate the mutation spectrum of the Fenton reaction-based oxidative renal tubular injury, and found that the major mutations consist of large-size deletions with short homologous sequences at the junctions and transversion-type point mutations at G:C base pairs. The mutant frequency was the highest at the first week of repeated Fe-NTA administration, as shown by the immunohistochemistry of 8-OHdG and acrolein-dA as well as the presence of these two modified bases at the *gpt* loci, indicating that this early stage is one of the critical periods in this Fenton reaction-induced carcinogenesis.

Acknowledgments

−53−

Table 2. Comparison of mutations induced by various mutagens in gpt delta transgenic mice

Target	Kidney†				Bone marrow[38]		Colon[39]	
	Control (MF = 1.0)	Fe-NTA-1 W (MF = 2.4)	Fe-NTA-2 W (MF = 1.4)	Fe-NTA-3 W (MF = 1.1)	Control (MF = 1.0)	PhIP (MF = 10.9)	Control (MF = 1.0)	ENU (MF = 3.2)
G:C–A:T	40%	28.6% (1.72)	8.7% (0.30)	16.7% (0.46)	43.1%	14.1%	26.9%	28.3%
A:T–G:C	10%	7.1% (1.70)	21.7% (3.04)	5.6% (0.62)	11.1%	0.0%	3.8%	20.0%
G:C–T:A	10%	10.7% (2.57)	8.7% (1.21)	0% (0.00)	26.4%	52.5%	11.5%	15.0%
G:C–C:G	10%	32.1% (7.70)	4.3% (0.60)	22.2% (2.44)	0.0%	13.1%	7.7%	0.0%
A:T–T:A	0%	3.6% (∞)	4.3% (∞)	11.1% (∞)	5.6%	1.0%	3.8%	28.3%
A:T–C:G	10%	7.1% (1.70)	17.4% (2.44)	11.1% (0.62)	4.2%	0.0%	0.0%	5.0%
Deletion	10%	7.1% (1.70)	26.1% (3.65)	22.2% (2.44)	4.2%	15.1%	38.5%	3.3%
Insertion	10%	3.6% (0.86)	4.3% (0.60)	11.1% (1.22)	5.6%	1.0%	7.7%	0.0%
Others	0%	0.0% (NA)	4.3% (∞)	0.0% (NA)	0.0%	3.0%	0.0%	0.0%

Target	Bone marrow[41]		Liver[53]		Liver[54]		Epidermis[55]		Liver[56]	
	Control (MF = 1.0)	MCC (MF = 2.9)	Control (MF = 1.0)	APNH (MF = 10.3)	Control (MF = 1.0)	γ-ray (MF = 3.2)	Control (MF = 1.0)	UVB (MF = 7.7)	Control (MF = 1.0)	MelQx (MF = 8.6)
G:C–A:T	24.1%	13.3%	41%	23%	27%	20%	64%	87%	43%	16%
A:T–G:C	3.4%	6.7%	10%	1%	15%	0%	0%	3%	8%	0%
G:C–T:A	31.0%	26.7%	14%	51%	12%	25%	9%	0%	10%	54%
G:C–C:G	10.3%	6.7%	2%	1%	4%	0%	0%	1%	4%	5%
A:T–T:A	6.9%	3.3%	8%	0%	4%	0%	9%	4%	8%	3%
A:T–C:G	10.3%	3.3%	4%	0%	23%	10%	10%	0%	2%	0%
Deletion	13.8%	6.7%	18%	16%	12%	35%	18%	0%	12%	16%
Insertion	0.0%	0.0%	2%	0%	4%	10%	0%	0%	2%	0%
Others	0.0%	33.3%	2%	7%	0%	0%	0%	5%	11%	6%

†present study. The number in parenthesis is the relative mutation frequency in comparison to the untreated control. MF, mutation frequency; NA, not applied; W, week(s); Fe-NTA, ferric nitrilotriacetate; PhIP, 2-amino-1-methyl-6-phenylimidazo [4,5-b]pyridine; ENU, ethylnitrosourea; MMC, mitomycin C; APNH, aminophenylnorharman; UVB, ultraviolet B; MelQx, 2-amino-3,8-dimethylimidazo[4,5-f]quinoxaline.

References

1 Halliwell B, Gutteridge JMC. Free radicals in biology and medicine. Oxford: Clarendon Press, 1999.
2 Iuchi K, Ichimiya A, Akashi A et al. Non-Hodgkin's lymphoma of the pleural cavity developing from long-standing pyothorax. Cancer 1987; 60: 1771–5.
3 Gilmour P, Brown D, Beswick P, MacNee W, Rahman I, Donaldson K. Free radical activity of industrial fibers: role of iron in oxidative stress and activation of transcription factors. Environ Health Perspect 1997; 105 (Suppl 5): 1313–17.
4 Hodgson J, Darnton A. The quantitative risks of mesothelioma and lung cancer in relation to asbestos exposure. Ann Occup Hyg 2000; 44: 565–601.
5 Uemura N, Okamoto S, Yamamoto S et al. Helicobacter pylori infection and the development of gastric cancer. N Engl J Med 2001; 345: 784–9.
6 Naito Y, Yoshikawa T. Carcinogenesis and chemoprevention in gastric cancer associated with helicobacter pylori infection: role of oxidants and antioxidants. J Clin Biochem Nutr 2005; 36: 37–49.
7 Collins R, Feldman M, Fordtran J. Colon cancer, dysplasia, and surveillance in patients with ulcerative colitis. A critical review. N Engl J Med 1987; 316: 1654–8.
8 Eaden J, Abrams K, Mayberry J. The risk of colorectal cancer in ulcerative colitis: a meta-analysis. Gut 2001; 48: 526–35.
9 Toyokuni S. Iron-induced carcinogenesis: the role of redox regulation. Free Radic Biol Med 1996; 20: 553–66.
10 Elmberg M, Hultcrantz R, Ekbom A et al. Cancer risk in patients with hereditary hemochromatosis and in their first-degree relatives. Gastroenterology 2003; 125: 1733–41.
11 Grodstein F, Speizer F, Hunter D. A prospective study of incident squamous cell carcinoma of the skin in the nurses' health study. J Natl Cancer Inst 1995; 87: 1061–6.
12 Nishigori C, Hattori Y, Toyokuni S. Role of reactive oxygen species in skin carcinogenesis. Antioxid Redox Signal 2004; 6: 561–70.
13 Preston D, Kusumi S, Tomonaga M et al. Cancer incidence in atomic bomb survivors. Part III. Leukemia, lymphoma and multiple myeloma, 1950–87. Radiat Res 1994; 137: S68–97.
14 Li JL, Okada S, Hamazaki S, Ebina Y, Midorikawa O. Subacute nephrotoxicity and induction of renal cell carcinoma in mice treated with ferric nitrilotriacetate. Cancer Res 1987; 47: 1867–9.

15 Ebina Y, Okada S, Hamazaki S, Ogino F, Li JL, Midorikawa O. Nephrotoxicity and renal cell carcinoma after use of iron- and aluminum-nitrilotriacetate complexes in rats. J Natl Cancer Inst 1986; 76: 107–13.
16 Nishiyama Y, Suwa H, Okamoto K, Fukumoto M, Hiai H, Toyokuni S. Low incidence of point mutations in H-, K- and N-ras oncogenes and p53 tumor suppressor gene in renal cell carcinoma and peritoneal mesothelioma of Wistar rats induced by ferric nitrilotriacetate. Jpn J Cancer Res 1995; 86: 1150–8.
17 Toyokuni S, Mori T, Dizdaroglu M. DNA base modifications in renal chromatin of Wistar rats treated with a renal carcinogen, ferric nitrilotriacetate. Int J Cancer 1994; 57: 123–8.
18 Toyokuni S, Uchida K, Okamoto K, Hattori-Nakakuki Y, Hiai H, Stadtman ER. Formation of 4-hydroxy-2-nonenal-modified proteins in the renal proximal tubules of rats treated with a renal carcinogen, ferric nitrilotriacetate. Proc Natl Acad Sci USA 1994; 91: 2616–20.
19 Toyokuni S, Luo XP, Tanaka T, Uchida K, Hiai H, Lehotay DC. Induction of a wide range of C_{2-12} aldehydes and C_{7-12} acyloins in the kidney of Wistar rats after treatment with a renal carcinogen, ferric nitrilotriacetate. Free Radic Biol Med 1997; 22: 1019–27.
20 Zhang D, Okada S, Yu Y, Zheng P, Yamaguchi R, Kasai H. Vitamin E inhibits apoptosis, DNA modification, and cancer incidence induced by iron-mediated peroxidation in Wistar rat kidney. Cancer Res 1997; 57: 2410–14.
21 Tanaka T, Iwasa Y, Kondo S, Hiai H, Toyokuni S. High incidence of allelic loss on chromosome 5 and inactivation of $p15^{INK4B}$ and $p16^{INK4A}$ tumor suppressor genes in oxystress-induced renal cell carcinoma of rats. Oncogene 1999; 18: 3793–7.
22 Hiroyasu M, Ozeki M, Kohda H et al. Specific allelic loss of $p16^{INK4A}$ tumor suppressor gene after weeks of iron-mediated oxidative damage during rat renal carcinogenesis. Am J Pathol 2002; 160: 419–24.
23 Tanaka T, Akatsuka S, Ozeki M, Shirase T, Hiai H, Toyokuni S. Redox regulation of annexin 2 and its implications for oxidative stress-induced renal carcinogenesis and metastasis. Oncogene 2004; 23: 3980–9.
24 Dutta KKN, Ishinaka Y, Masutani H et al. Thioredoxin-binding protein-2 is a target gene in oxidative stress-induced renal carcinogenesis. Lab Invest 2005; 85: 798–807.
25 Nakatsuka S, Tanaka H, Namba M. Mutagenic effects of ferric nitrilotriacetate (Fe-NTA) on V79 Chinese hamster cells and its inhibitory effects on cell-cell communication. Carcinogenesis 1990; 11: 257–60.

–54–

26 Toyokuni S, Sagripanti JL, Hitchins VM. Cytotoxic and mutagenic effects of ferric nitrilotriacetate on L5178Y mouse lymphoma cells. *Cancer Lett* 1995; 88: 157–62.

27 Gossen J, de Leeuw W, Tan C *et al.* Efficient rescue of integrated shuttle vectors from transgenic mice: a model for studying mutations in vivo. *Proc Natl Acad Sci USA* 1989; 86: 7971–5.

28 Kohler S, Provost G, Fieck A *et al.* Spectra of spontaneous and mutagen-induced mutations in the *lacI* gene in transgenic mice. *Proc Natl Acad Sci USA* 1991; 88: 7958–62.

29 Gondo Y, Shioyama Y, Nakao K, Katsuki M. A novel positive detection system of in vivo mutations in *rpsL* (*strA*) transgenic mice. *Mutat Res* 1996; 360: 1–14.

30 Nohmi T, Katoh M, Suzuki H *et al.* A new transgenic mouse mutagenesis test system using Spi⁻ and 6-thioguanine selections. *Environ Mol Mutagen* 1996; 28: 465–70.

31 Nohmi T, Masumura K. Molecular nature of intrachromosomal deletions and base substitutions induced by environmental mutagens. *Environ Mol Mutagen* 2005; 45: 150–61.

32 Toyokuni S, Tanaka T, Hattori Y *et al.* Quantitative immunohistochemical determination of 8-hydroxy-2'-deoxyguanosine by a monoclonal antibody N45.1: its application to ferric nitrilotriacetate-induced renal carcinogenesis model. *Lab Invest* 1997; 76: 365–74.

33 Kawai Y, Furuhata A, Toyokuni S, Aratani Y, Uchida K. Formation of acrolein-derived 2'-deoxyadenosine adduct in an iron-induced carcinogenesis model. *J Biol Chem* 2003; 278: 50 346–54.

34 Toyokuni S, Akatsuka S, Aung TT, Dutta KK. Free radical-induced carcinogenesis: target genes and fragile genome sites. *Free Radic Res* 2005; 39 (Suppl 1): S30.

35 Akatsuka S, Aung TT, Dutta KK *et al.* Contrasting genome-wide distribution of 8-hydroxyguanine and acrolein-modified adenine during oxidative stress-induced renal carcinogenesis. *Am J Pathol* 2006, in press.

36 Nakae D, Mizumoto Y, Kobayashi E, Noguchi O, Konishi Y. Improved genomic/nuclear DNA extraction for 8-hydroxydeoxyguanosine analysis of small amounts of rat liver tissue. *Cancer Lett* 1995; 97: 233–9.

37 Ono T, Miyamura Y, Ikehata H *et al.* Spontaneous mutant frequency of *lacZ* gene in spleen of transgenic mouse increases with age. *Mutat Res* 1995; 338: 183–8.

38 Masumura K, Matsui K, Yamada M *et al.* Mutagenicity of 2-amino-1-methyl-6-phenylimidazo [4,5-b]pyridine (PhIP) in the new *gpt* delta transgenic mouse. *Cancer Lett* 1999; 143: 241–4.

39 Masumura K, Matsui M, Katoh M *et al.* Spectra of *gpt* mutations in ethylnitrosourea-treated and untreated transgenic mice. *Environ Mol Mutagen* 1999; 34: 1–8.

40 Nohmi T, Suzuki T, Masumura K. Recent advances in the protocols of transgenic mouse mutation assays. *Mutat Res* 2000; 455: 191–215.

41 Takeiri A, Mishima M, Tanaka K *et al.* Molecular characterization of mitomycin C-induced large deletions and tandem-base substitutions in the bone marrow of *gpt* delta transgenic mice. *Chem Res Toxicol* 2003; 16: 171–9.

42 Cariello N, Piegorsch W, Adams W, Skopek T. Computer program for the analysis of mutational spectra: application to *p53* mutations. *Carcinogenesis* 1994; 15: 2281–5.

43 Shibata A, Masutani M, Kamada N *et al.* Efficient method for mapping and characterizing structures of deletion mutations in *gpt* delta mice using Southern blot analysis with oligo DNA probes. *Environ Mol Mutagen* 2004; 43: 204–7.

44 Hamazaki S, Okada S, Ebina Y, Midorikawa O. Acute renal failure and glucosuria induced by ferric nitrilotriacetate in rats. *Toxicol Appl Pharmacol* 1985; 77: 267–74.

45 Toyokuni S, Akatsuka S. What has been learned from the studies of oxidative stress-induced carcinogenesis: proposal of the concept of oxygenomics. *J Clin Biochem Nutr* 2006; 39: 3–10.

46 Shibutani S, Takeshita M, Grollman AP. Insertion of specific bases during DNA synthesis past the oxidation-damaged base 8-oxodG. *Nature* 1991; 349: 431–4.

47 Kasai H. Analysis of a form of oxidative DNA damage, 8-hydroxy-2'-deoxyguanosine, as a marker of cellular oxidative stress during carcinogenesis. *Mutat Res* 1997; 387: 147–63.

48 Nakabeppu Y. Regulation of intracellular localization of human MTH1, OGG1, and MYH proteins for repair of oxidative DNA damage. *Prog Nucl Acid Res Mol Biol* 2001; 68: 75–94.

49 Steenken S. Purine bases, nucleosides, and nucleotides: aqueous solution redox chemistry and transformation reactions of their radical reactions and e⁻ and. OH adducts. *Chem Rev* 1989; 89: 503–20.

50 Dizdaroglu M. Chemical determination of free radical-induced damage to DNA. *Free Radic Biol Med* 1991; 10: 225–42.

51 Ober M, Muller H, Pieck C, Gierlich J, Carell T. Base pairing and replicative processing of the formamidopyrimidine-dG DNA lesion. *J Am Chem Soc* 2005; 127: 18 143–9.

52 Hayashi H, Kondo H, Masumura K, Shindo Y, Nohmi T. Novel transgenic rat for in vivo genotoxicity assays using 6-thioguanine and Spi⁻ selection. *Environ Mol Mutagen* 2003; 41: 253–9.

53 Masumura K, Totsuka Y, Wakabayashi K, Nohmi T. Potent genotoxicity of aminophenylnorharman, formed from non-mutagenic norharman and aniline, in the liver of *gpt* delta transgenic mouse. *Carcinogenesis* 2003; 24: 1985–93.

54 Masumura K, Kuniya K, Kurobe T, Fukuoka M, Yatagai F, Nohmi T. Heavy-ion-induced mutations in the *gpt* delta transgenic mouse: comparison of mutation spectra induced by heavy-ion, X-ray, and gamma-ray radiation. *Environ Mol Mutagen* 2002; 40: 207–15.

55 Horiguchi M, Masumura K, Ikehata H *et al.* UVB-induced *gpt* mutations in the skin of *gpt* delta transgenic mice. *Environ Mol Mutagen* 1999; 34: 72–9.

56 Masumura K, Horiguchi M, Nishikawa A *et al.* Low dose genotoxicity of 2-amino-3,8-dimethylimidazo[4,5-f]quinoxaline (MeIQx) in *gpt* delta transgenic mice. *Mutat Res* 2003; 541: 91–102.

Combined genotoxic effects of radiation and a tobacco-specific nitrosamine in the lung of *gpt* delta transgenic mice

Megumi Ikeda [a,b], Ken-ichi Masumura [a], Yasuteru Sakamoto [a], Bing Wang [c], Mitsuru Nenoi [c], Keiko Sakuma [b], Isamu Hayata [c], Takehiko Nohmi [a,*]

[a] *Division of Genetics and Mutagenesis, National Institute of Health Sciences, 1-18-1 Kamiyoga, Setagaya-ku, Tokyo 158-8501, Japan*
[b] *Graduate School of Nutrition and Health Sciences, Kagawa Nutrition University, 3-9-21 Chiyoda, Sakado-shi, Saitama 350-0288, Japan*
[c] *Radiation Effect Mechanisms Research Group, Research Center of Radiation Protection, National Institute of Radiological Sciences, 4-9-1 Anagawa, Inage-ku, Chiba-shi, Chiba 263-8555, Japan*

Abstract

It is important to evaluate the health effects of low-dose-rate or low-dose radiation in combination with chemicals as humans are exposed to a variety of chemical agents. Here, we examined combined genotoxic effects of low-dose-rate radiation and 4-(methylnitrosamino)-1-(3-pyridyl)-1-butanone (NNK), the most carcinogenic tobacco-specific nitrosamine, in the lung of *gpt* delta transgenic mice. In this mouse model, base substitutions and deletions can be separately analyzed by *gpt* and Spi⁻ selections, respectively. Female *gpt* delta mice were either treated with γ-irradiation alone at a dose rate of 0.5, 1.0 or 1.5 mGy/h for 22 h/day for 31 days or combined with NNK treatments at a dose of 2 mg/mouse/day, i.p. for four consecutive days in the middle course of irradiation. In the *gpt* selection, the NNK treatments enhanced the mutation frequencies (MFs) significantly, but no obvious combined effects of γ-irradiation were observable at any given radiation dose. In contrast, NNK treatments appeared to suppress the Spi⁻ large deletions. In the Spi⁻ selection, the MFs of deletions more than 1 kb in size increased in a dose-dependent manner. When NNK treatments were combined, the dose–response curve became bell-shaped where the MF at the highest radiation dose decreased substantially. These results suggest that NNK treatments may elicit an adaptive response that eliminates cells bearing radiation-induced double-strand breaks in DNA. Possible mechanisms underlying the combined genotoxicity of radiation and NNK are discussed, and the importance of evaluation of combined genotoxicity of more than one agent is emphasized.
© 2006 Elsevier B.V. All rights reserved.

Keywords: Combined genotoxic effects; Radiation; NNK; Lung cancer; *gpt* delta mice; Deletion

1. Introduction

Environmental factors play important roles in the etiology of human cancer [1]. Of various environmental hazardous compounds, cigarette smoke is the most causative factor associated with the increase in cancer risk in humans. Tobacco smoking plays a major role in the etiology of lung, oral cavity and esophageal cancers, and a variety of chronic degenerative diseases [2]. Although cigarette smoke is a mixture of about 4000 chemicals including more than 60 known human carcinogens, 4-(methylnitrosamino)-1-(3-pyridyl)-1-butanone (nicotine-derived nitrosamino ketone, NNK) is the most carcinogenic tobacco-specific nitrosamine [3,4]. NNK induces lung tumors in mice,

* Corresponding author. Tel.: +81 3 3700 9873;
fax: +81 3 3707 6950.
E-mail address: nohmi@nihs.go.jp (T. Nohmi).

rats and hamsters, and International Agency for Research on Cancer has concluded that exposure to NNK and NNN (*N'*-nitrosonornicotine) is carcinogenic to humans [5]. NNK is metabolically activated by CYP (P-450) enzymes in the lung and generates O^6-methylguanine in DNA, which leads to G:C to A:T mutations, and the subsequent activation of Ki-*ras* proto-oncogene, an initiation of tumor development [6,7].

Radiation, on the other hand, is one of the most causative physical factors that induce human cancer. Radiation induces double-strand breaks (DSBs) in DNA, which lead to chromosome aberrations and cell deaths, and generates a variety of oxidative DNA damage [8]. Because of the genotoxicity, radiation at high doses clearly induces various tumors in humans [9]. Even at low doses, residential exposure to radioactive radon and its decay products may account for about 10% of all lung cancer deaths in the United States and about 20% of the lung cancer cases in Sweden [10,11].

Since humans are exposed to a variety of chemical and physical agents that may induce cancer, these factors may interact with each other and the action of one agent may be influenced by exposure to another agent [12]. The risk from combined exposure to more than one agent may be substantially higher or lower than predicted from the sum of the individual agents. In fact, low-dose radiation can induce an adaptive response, causing rodent or human cells to become resistant to genotoxic damage by subsequent higher doses of radiation [13]. Pre-exposure to alkylating agents at low doses induces another adaptive response that provides mechanisms by which the exposed bacterial cells can tolerate the higher challenging doses of genotoxic agents [14]. In addition, mitomycin C, bleomycin, hydrogen peroxide, metals and quercetin may also induce an adaptive response [15].

To explore the mechanisms underlying the interactive effects of chemical and physical agents on carcinogenesis, we examined the combined genotoxic effects of NNK and γ-irradiation in the lung of *gpt* delta transgenic mice [16]. In this mouse model, point mutations and deletions are separately analyzable by *gpt* and Spi⁻ selections, respectively [17]. Point mutations such as base substitutions are induced by a number of chemical carcinogens including NNK [18]. Spi⁻ selection detects deletions in size between 1 bp and 10 kb [19]. Deletions in size more than 1 kb, which we call large deletions in this study, are efficiently induced by γ-ray, X-ray and carbon-ion irradiation [20], and are thought to be generated by non-homologous end joining (NHEJ) of DSBs in DNA [21].

We report here that low-dose-rate γ-irradiation enhanced the mutation frequencies (MFs) of the large deletions in the lung of *gpt* delta mice in a dose-dependent manner. When combined with NNK treatments, however, the MF at the highest radiation dose, i.e., 1.02 Gy, was reduced by more than 50%, suggesting that NNK treatments may induce an adaptive response against radiation-induced deletion mutations. We discuss possible mechanisms of the adaptive response and emphasize the importance of the risk assessment of combined genotoxic effects of radiation and chemicals in vivo.

2. Materials and methods

2.1. Treatment of mice

gpt delta C57BL/6J transgenic mice were maintained in the conventional animal facility of National Institute of Radiological Sciences, Chiba, Japan, according to the institutional animal care guidelines. They were housed in autoclaved aluminum cages with sterile wood chips for bedding and given free access to standard laboratory chow (MB-1, Funabashi Farm Co., Japan) and acidified water under controlled lighting (12 h light/dark cycle). Seven-week-old female *gpt* delta mice were divided to eight groups each consisting of six mice. Three groups were γ-irradiated at a dose rate of 0.5, 1.0 or 1.5 mGy/h for 22 h/day for 2 weeks (Fig. 1). After the irradiation, three groups of mice were treated with a single i.p. injection of NNK (Toronto Research Chemicals, Toronto, Canada) dissolved in saline at a daily dose of 2 mg/mouse for four consecutive days. The irradiation continued during the 4-day treatments, and the mice were kept in the cage for another 2 weeks with irradiation. Three control groups were γ-irradiated as described but received saline instead of NNK. The whole irradiation period was 31 days, and the total estimated doses were 0.34, 0.68 and 1.02 Gy, respectively. Another control group of mice was treated with NNK as described but without γ-irradiation. The third control was kept in the cage for 31 days without γ-irradiation or NNK treatments. The source of radiation was ¹³⁷Cs, and the dose rate was estimated by a fluorescent glass dosimeter. The non-irradiated control groups were placed behind a concrete wall of 1 m thickness. The mice were sacrificed by cervical vertebral dislocation. The liver and lung were removed, placed immediately in liquid nitrogen, and stored at −80 °C until analysis.

2.2. DNA isolation and in vitro packaging of DNA

High-molecular-weight genomic DNA was extracted from the lung and the liver using the RecoverEase DNA Isolation Kit (Stratagene, La Jolla, CA). Lambda EG10 phages were rescued using Transpack Packaging Extract (Stratagene, La Jolla, CA).

2.3. gpt mutation assay

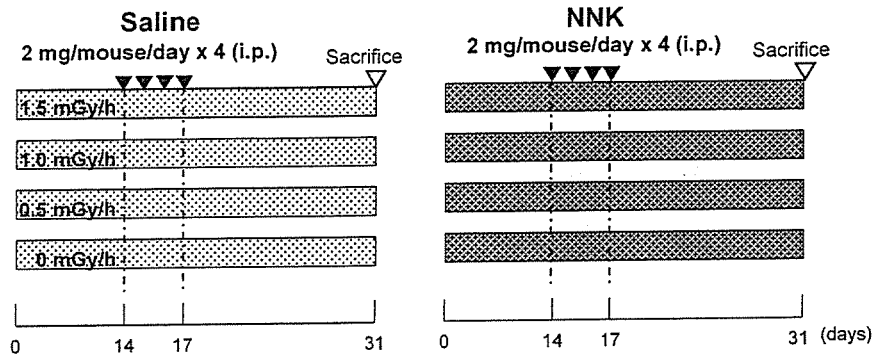The *gpt* mutagenesis assay was performed according to previously described methods [17]. Briefly, *Escherichia coli*

Fig. 1. An experimental design to examine the combined genotoxicity of γ-irradiation and NNK treatments in the lung of mice. Female 7-week-old *gpt* delta mice were divided into eight groups each composed of six mice. Three groups of mice were irradiated at a dose rate of 0.5, 1.0 or 1.5 mGy/h for 22 h/day for 14 days and treated with NNK at a daily dose of 2 mg/mouse for four consecutive days. The irradiation continued during the NNK treatments and the following 14 days before sacrifice. The total radiation doses were 0.34, 0.68 and 1.02 Gy, respectively. Control three groups of mice were γ-irradiated but without NNK treatments. Another control group was treated with NNK but without γ-irradiation. The third control was kept in the cage for 31 days without γ-irradiation or NNK treatments. Transgene λEG10 DNA was rescued from the lung of mice, and the base substitutions and deletions were analyzed by *gpt* and Spi⁻ selection, respectively.

YG6020 expressing Cre recombinase was infected with the rescued phage. The bacteria were then spread onto M9 salts plates containing chloramphenicol (Cm) and 6-thioguanien (6-TG), and incubated for 72 h at 37 °C for selection for the colonies harboring a plasmid carrying the Cm acetyltransferase (*cat*) gene and a mutated *gpt* gene. The 6-TG-resistant colonies were streaked again onto the same selection plates for confirmation of the resistant phenotype. All the confirmed *gpt* mutants recovered from the lung were sequenced and the identical mutations from the same mouse counted one mutant. The *gpt* MFs in the lung were calculated by dividing the number of the *gpt* mutants after sequencing by the number of rescued plasmids, which was estimated from the number of colonies on plates containing Cm but without 6-TG. Since no *gpt* mutants recovered from the liver were sequenced, the MFs in the liver were calculated by dividing the number of confirmed 6-TG-resistant colonies by the number of rescued plasmids.

2.4. PCR and DNA sequencing analysis of 6-TG-resistant mutants

A 739 bp DNA fragment containing the *gpt* gene was amplified by polymerase chain reaction (PCR) using primers 1 and 2 [17]. The reaction mixture contained 5 pmol of each primer and 200 mM of each dNTP. PCR amplification was carried out using Ex Taq DNA polymerase (Takara Bio, Shiga, Japan) and performed with a Model PTC-200 Thermal Cycler (MJ Research, Waltham, MA). PCR products were analyzed by agarose gel electrophoresis to determine the amount of the products. DNA sequencing of the *gpt* gene was performed with BigDye™ Terminator Cycle Sequencing Kit (Applied Biosystems, Foster City, CA) using sequencing primer gptA2 (5′-TCTCGCGCAACCTATTTTCCC-3′). The sequencing reaction products were analyzed on an Applied Biosystems model 310 genetic analyzer (Applied Biosystems, Foster City, CA).

2.5. Spi⁻ mutation assay

The Spi⁻ assay was performed as described previously [17]. The lysates of Spi⁻ mutants were obtained by infection of *E. coli* LE392 with the recovered Spi⁻ mutants. The lysates were used as templates for PCR analysis to determine the deleted regions. Sequence changes in the *gam* and *redAB* genes, and the outside of the *gam/redAB* genes were identified by DNA sequencing analysis [22]. The appropriate primers for DNA sequencing were selected based on the results of PCR analysis. The entire sequence of λEG10 is available at http://dgm2alpha.nhis.go.jp.

2.6. Statistical analysis

All data are expressed as mean ± standard deviations of the MFs of six mice for lung and those of four mice for liver. Differences between groups were tested for statistical significance using a Student's *t*-test. A *p* value less than 0.05 denoted the presence of a statistically significant difference.

3. Result

3.1. gpt MFs in the lung of NNK-treated and γ-irradiated gpt delta mice

We measured the *gpt* MFs in the lung of *gpt* delta mice untreated or treated with NNK in the absence or the presence of γ-irradiation (Fig. 2). NNK treatments significantly enhanced the MFs over the control groups. The mean MFs ($\times 10^{-6}$) of NNK-treated versus saline-treated groups were 14.3 ± 6.9 versus 4.2 ± 4.0, 20.7 ± 5.1 versus 4.7 ± 3.0, 15.2 ± 7.3 versus 2.0 ± 2.1 and 17.2 ± 7.9 versus 2.7 ± 1.4 at the dose rates of 0, 0.5, 1.0 and 1.5 mGy/h, respectively. The γ-irradiation
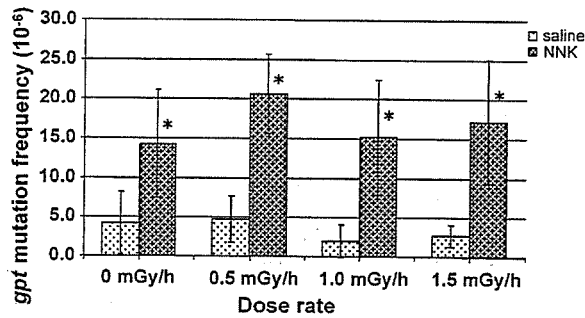
Fig. 2. *gpt* MFs in the lung of mice untreated or treated with NNK in the absence or the presence of γ-irradiation. An asterisk (*) denotes $p < 0.05$ ($n = 6$) in a Student's t-test of MF of NNK-treated vs. the corresponding untreated mice. Vertical bars show the standard deviations with mice as the unit of comparison.

alone, i.e., the saline-treated group, did not enhance the *gpt* MF under the conditions. Hence, the increases in MFs are due to NNK treatments. Although the individual MFs slightly varied, there was no significant difference among the four MFs of the NNK-treated groups. Thus, we suggested that the irradiation did not modify the genotoxicity of NNK in the lung of mice.

To confirm the results in the lung, we analyzed the *gpt* MFs in the liver of the NNK-treated and saline-treated groups. The mean MFs ($\times 10^{-6}$) of NNK-treated versus saline-treated groups were 134 ± 48 versus 8.1 ± 3.8, 105 ± 31 versus 8.7 ± 3.5, 101 ± 18 versus 8.0 ± 4.2 and 128 ± 76 versus 6.8 ± 0.6 at the dose rates of 0, 0.5, 1.0 and 1.5 mGy/h, respectively. Although NNK treatments induced mutations much more strongly in the liver than in the lung, there were no significant modulating effects of radiation on the NNK-induced mutations in the liver.

The irradiation might modulate specific types of mutations without affecting the total *gpt* MFs. To exam-

ine the possibility, we determined the mutation spectra of the *gpt* gene in the lung and examined whether the radiation affected specific types of mutations (Table 1). NNK treatments induced G:C to A:T, G:C to T:A, A:T to T:A and A:T to C:G mutations. In particular, A:T to T:A mutations were induced more than 20-fold by NNK treatments. We observed, however, no remarkable variations of mutation spectra associated with the dose rates of combined radiation. Thus, we concluded that the irradiation did not enhance or suppress the base substitutions induced by NNK in the lung of *gpt* delta mice significantly.

3.2. Spi⁻ MFs in the lung of NNK-treated and γ-irradiated gpt delta mice

Next, we measured the Spi⁻ MFs in the lung of *gpt* delta mice untreated or treated with NNK in the absence or the presence of γ-irradiation. The mean Spi⁻ MFs ($\times 10^{-6}$) of NNK-treated versus saline-treated groups were 5.15 ± 2.34 versus 4.11 ± 0.98, 5.47 ± 1.98 versus 5.06 ± 3.50, 5.36 ± 1.56 versus 4.09 ± 0.80 and 5.39 ± 2.56 versus 4.65 ± 1.78 at the dose rates of 0, 0.5, 1.0 and 1.5 mGy/h, respectively. These results suggest that neither NNK treatments nor the irradiation enhanced the Spi⁻ MFs in the lung significantly.

To investigate the combined effects of NNK and γ-irradiation on specific types of deletion mutations, we identified all the Spi⁻ mutations by DNA sequencing analysis (Table 2). Of various classes of deletions observed, only the MFs of large deletions in the size of more 1 kb increased in a dose-dependent manner in the saline-treated group. To examine the dose–response in more detail, we determined the MFs of the large deletions
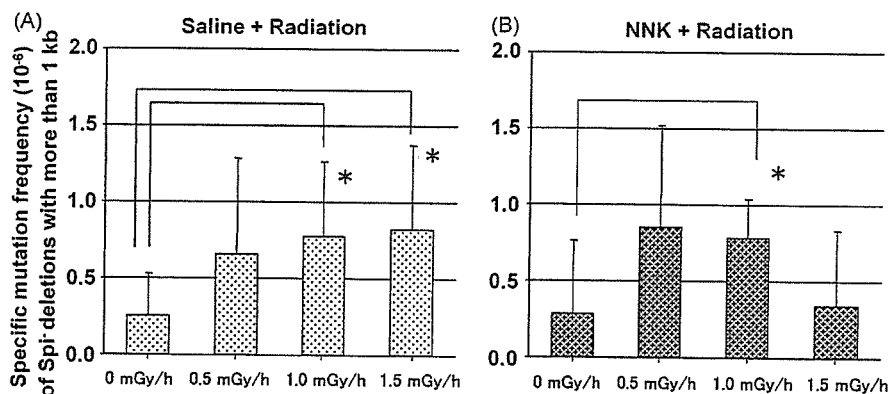
Fig. 3. Specific MF of large deletions with the size of more than 1 kb in the lung of unirradiated or γ-irradiated mice. The mice were not treated (A) or treated with NNK (B). An asterisk (*) denotes $p < 0.05$ ($n = 5$) in a Student's t-test of MF of γ-irradiated vs. the corresponding unirradiated mice. Vertical bars show the standard deviations with mice as the unit of comparison.

Table 1

gpt mutation spectra in the lung of NNK-treated and γ-irradiated gpt delta mice

Treatment: saline	0 mGy/h			0.5 mGy/h			1.0 mGy/h			1.5 mGy/h		
	No.	MF ($\times 10^{-6}$)	%	No.	MF ($\times 10^{-6}$)	%	No.	MF ($\times 10^{-6}$)	%	No.	MF ($\times 10^{-6}$)	%
Base substitution												
Transition												
G:C → A:T	15 (6)	1.81	43	12 (6)	1.76	38	5 (2)	0.61	29	8 (4)	0.81	30
A:T → G:C	2	0.24	6	4	0.59	13	1	0.12	6	2	0.20	7
Transversion												
G:C → T:A	1	0.12	3	5 (2)	0.73	16	1	0.12	6	6 (1)	0.61	22
G:C → C:G	1	0.12	3	0	0.00	0	0	0.00	0	2 (2)	0.20	7
A:T → T:A	1	0.12	3	1	0.15	3	1	0.12	6	1	0.10	4
A:T → C:G	3	0.36	9	1	0.15	3	1	0.12	6	1	0.10	4
Deletion	8	0.97	23	6	0.88	19	7	0.85	41	6	0.61	22
−1 bp	3			2			5			3		
>2 bp	5			4			2			3		
Insertion	3	0.36	9	3	0.44	9	1	0.12	6	1	0.10	4
Others	1	0.12	3	0	0.00	0	0	0.00	0	0	0.00	0
	35	4.23	100	32	4.69	100	17	2.06	100	27	2.73	100

Treatment: NNK	0 mGy/h			0.5 mGy/h			1.0 mGy/h			1.5 mGy/h		
	No.	MF ($\times 10^{-6}$)	%	No.	MF ($\times 10^{-6}$)	%	No.	MF ($\times 10^{-6}$)	%	No.	MF ($\times 10^{-6}$)	%
Base substitution												
Transition												
G:C → A:T	24 (2)	5.11	36	45 (8)	8.02	39	32 (5)	5.85	39	54 (6)	8.51	50
A:T → G:C	0	0.00	0	7	1.25	6	6	1.10	7	2	0.32	2
Transversion												
G:C → T:A	9 (2)	1.92	13	10 (1)	1.78	9	7 (1)	1.28	8	7 (1)	1.10	6
G:C → C:G	0	0.00	0	2	0.36	2	0	0.00	0	3	0.47	3
A:T → T:A	13	2.77	19	26	4.64	22	17	3.11	21	17 (1)	2.68	16
A:T → C:G	15	3.19	22	12	2.14	10	8	1.46	10	12 (1)	1.89	11
Deletion	5	1.06	8	12	2.14	10	9	1.65	11	12	1.89	11
−1 bp	5			6			4			5		
>2 bp	0			6			5			7		
Insertion	1	0.21	2	0	0.00	0	4	0.73	5	1	0.16	1
Others	0	0.00	0	2	0.36	2	0	0.00	0	1	0.16	1
	67	14.26	100	116	20.68	100	83	15.18	100	109	17.18	100

No. stands for the number of mutations.

of each mouse and calculated the mean MF and standard derivations. The mean MFs ($\times 10^{-6}$) and standard derivations were 0.25 ± 0.28, 0.66 ± 0.63, 0.77 ± 0.49 and 0.82 ± 0.55 at the dose rates of 0, 0.5, 1.0 and 1.5 mGy/h, respectively (Fig. 3A). The values at 1.0 and 1.5 mGy/h were about three-fold higher than the value at 0 mGy/h, and the differences were statistically

significant ($p = 0.04$). In contrast, the dose–response curve of large deletions in NNK-treated group was a bell shaped (Fig. 3B). The mean MFs ($\times 10^{-6}$) and standard derivations of large deletions in the NNK-treated group were 0.29 ± 0.47, 0.85 ± 0.66, 0.78 ± 0.26 and 0.35 ± 0.48 at the dose rates of 0, 0.5, 1.0 and 1.5 mGy/h, respectively. It should be noted that the

Table 2

Spi$^-$ mutation spectra in the lung of NNK-treated and γ- irradiated *gpt* delta mice

Treatment: saline	0 mGy/h			0.5 mGy/h			1.0 mGy/h			1.5 mGy/h		
	No.	MF ($\times 10^{-6}$)	%	No.	MF ($\times 10^{-6}$)	%	No.	MF ($\times 10^{-6}$)	%	No.	MF ($\times 10^{-6}$)	%
1 bp deletion												
Simple												
Guanine	9	0.49	12	7	0.59	12	5	0.34	8	4	0.30	7
Adenine	4	0.22	5	0	0.00	0	2	0.14	3	1	0.08	2
In run												
Guanine	13	0.71	17	15	1.27	25	12	0.82	20	13	0.99	21
Adenine	31	1.70	41	19	1.60	32	22	1.50	37	25	1.91	41
With b.s.	0	0.00	0	0	0.00	0	0	0.00	0	0	0.00	0
>2 bp deletion	15	0.82	20	17	1.43	28	17	1.16	28	13	0.99	21
2 bp ∼ 1 kb	2	0.11	3	7	0.59	12	3	0.20	5	1	0.08	2
>1 kb	5	*0.27*	7	7	*0.59*	12	11	*0.75*	18	10	*0.76*	16
Complex	8	0.44	11	3	0.25	5	3	0.20	5	2	0.15	3
Insertion	3	0.16	4	2	0.17	3	2	0.14	2	5	0.38	8
	75	4.11	100	60	5.06	100	60	4.09	100	61	4.65	100

Treatment: NNK	0 mGy/h			0.5 mGy/h			1.0 mGy/h			1.5 mGy/h		
	No.	MF ($\times 10^{-6}$)	%	No.	MF ($\times 10^{-6}$)	%	No.	MF ($\times 10^{-6}$)	%	No.	MF ($\times 10^{-6}$)	%
1 bp deletion												
Simple												
Guanine	5	0.61	12	4	0.46	8	4	0.50	9	4	0.48	9
Adenine	3	0.37	7	0	0.00	0	4	0.50	9	1	0.12	2
In run												
Guanine	9	1.10	21	19	2.17	40	9	1.12	21	14	1.68	31
Adenine	12	1.47	29	10	1.14	21	9	1.12	21	15	1.80	33
With b.s.	0	0.00	0	0	0.00	0	2	0.25	5	0	0.00	0
>2 bp deletion	12	1.47	29	10	1.14	21	11	1.37	26	11	1.32	24
2 bp ∼ 1 kb	6	0.74	14	2	0.23	4	3	0.37	7	7	0.84	16
>1 kb	2	*0.25*	5	7	*0.80*	15	7	*0.87*	16	2	*0.24*	4
Complex	4	0.49	10	1	0.11	2	1	0.12	2	2	0.24	4
Insertion	1	0.12	2	5	0.57	10	4	0.50	9	0	0.00	0
	42	5.15	100	48	5.47	100	43	5.36	100	45	5.39	100

No. stands for the number of mutations. Specific MFs of large deletions more than 1 kb in size are italicised.

MF at 1.0 mGy/h (0.78×10^{-6}) was about three-fold higher than that of 0 mGy/h ($p = 0.04$) but the MF at 1.5 mGy/h (0.35×10^{-6}) was very similar to that of 0 mGy/h (0.29×10^{-6}). The p values of the differences of MFs between saline-treated and NNK-treated groups at dose rates of 0, 0.5, 1.0 and 1.5 mGy/h were 0.44, 0.32, 0.48 and 0.09, respectively. From the results, we suggested that NNK treatments suppressed the induc-

Fig. 4. Molecular nature of large deletions recovered from the lung of *gpt* delta mice untreated or treated with NNK in the absence or the presence of γ-irradiation. Horizontal bars represent the deleted regions of mutants. Most of the mutants lack the entire *gam* gene and part of the *redAB* genes, but some lack the *gam* gene and the upstream region. The *gam* and *redAB* genes make an operon and the transcription starts from the upstream of the *gam* gene. Short homologous sequences in the junctions of the mutants are underlined. Underlined sequences, i.e.. T or CTTA, in the middle of two sequences are inserted sequences in the junctions.

Deletion size (bp)	Sequence of the junction of deletion		No. of mutant	Mouse I.D.
Saline γ-ray (mG/h) 0				
-1242	TGAATGGTTCGCGGCGGC	GTGTTTGTGCATCCATCT	2	2,34
-2912	AGAGCAGGCGGTACGCAT	TAATCCTTAACTTTGCCC	1	34
-3393	GGTAAATCCGGCATGTAC	AGCCAGGGGATCTCTCCC	1	34
-7626	CAGCCAGCGTTGCGAGTG	CGGTTGCTTTATGCATGG	1	3
0.5				
-1608	GCTATCACGTTGTGAACT	TCGGATTTAGTGCGCTTT	2	9,11
-2912	AGAGCAGGCGGTACGCAT	TAATCCTTAACTTTGCCC	1	9
-3650	ACTGTTGGTTAATACGCT	AAAGCTCCAAGCTCAACA	1	41
-5339	GATGCGGCTAACGTATGA	TGCCTTTGCGGCTTGTAA	1	11
-5582÷1	CGCCTGTCTCTGCCTAAT T	ATACTCTCTAATCTTGGC	1	10
-6789	CATCCTGAACCCATTGAC	ACCACAGCGTGATGGGCT	1	10
1.0				
-1164	ATGGTTCGCGGCGGCATT	TTGCGCTTACCCCAACCA	1	50
-1922	CACTGAATCATGGCTTTA	AGAAGCAATAACCCGCAG	1	50
-3219	TTCTATTTCTGATGCTGA	GTATCACACACCCCAAAG	1	19
-3326	TGATGTATTGCTGGTTTC	CTGGTTTTGCGCTTACCC	1	19
-3360	GATTTCAGAATTAGCCTG	GGGTATCATGTAGCCGCT	1	49
-3473	GCGGCGTTTGATGTATTG	TGTGGCAGTTGTAGTCCT	1	19
-3966	TAACTTCCGGAGCCACAC	GAAGACGCGATCTCGCTC	1	17
-4716	TCCTTTGATGCGAATGCC	GCATAATTACTCCTGATA	1	18
-5053	AATTCATGGAAAAGGTCT	GCGTAAACTCCGCTGTCA	1	50
-5244	GTATCAGCAATGTTTATG	GTAGCTTGGCTTCTACCT	1	17
-6140	ATCGGGGATTCAGTAACA	CGCCTTCTGTCACCACCA	1	10
1.5				
-3645	GGTCTGCGTCAAATCCCC	GGTTATCTGTATGTTTTT	1	27
-3833	AATCGATGGTGTTACCAA	AACCCGGCGCTGAGGCCG	1	57
-3879	TTGCTGGTTTCTTTCCCG	CTGAGGCCGGGTTATTCT	1	27
-4014	TTTTCGATGAACTCCGGC	CTTACCGGGTTATCCCCA	1	26
-4035	CTTCCCAGCCAGCGTTGC	CCTGCACCAGCGTGGTAA	1	27
-4416	TAAAATAAATCCCCGCGA	TTGGCACATTGGCAGCTA	1	27
-5194	ATAACTCTGTTGAATGGC	ATATGATGACAATGTCGC	1	58
-5366	TAACGCAGATCGGATGAT	CCGCCAGTGGCGCACTAT	1	58
-5905	GGAACAGAGCGGCAATAA	CTGCCTGATTAGCGGCGA	1	25
-6629	CCGCAATTTCTTTTGTGG	CCTTCAACAAACAAAAAA	1	26
NNK γ-ray (mG/h) 0				
-4283	TGATGATGCGGGACCAGC	GACCACGCCTTTGGGGCG	1	38
-6283	TTGCCAGGCTTAAATGAG	ATCTAAGGCCGTCACCTG	1	5
0.5				
-1035	ATCACCTTTAAATGCCGT	AACCCCCCGCGATTGGCA	1	15
-1315	CAGTGCTTTAGCGTTAAC	ATAGCTGTGAAAATATCG	1	45
-2724	TGCTGGCCCCGTGGCGTT	CTCCAGCCCCTATCCCCC	1	45
-4318	CCTTTTTCCATGTCGTCT	CAGCGGGTACGGTTGGCG	1	13
-5146	CGAGAAGATGTTGAGCAA	TCTGCCAGTTCTGCCTCT	1	15
-5273	GCTGACGCCGCCTTGCCC	CCCGCGATTGGCACATTG	1	14
-9265	TGTGCCACGCATCATCCC	ATGGATGCAGCCTCCAGA	1	15
1.0				
-1373	GTGAGCAATGGTTTCAAC	TGGCGATAGTGGGTATCA	1	23
-3466	AGGATTCATTGTCCTGCT	GTTCGCCACCCAACCCGC	1	53
-5445	GTTTAACATGCCGATTGC	AGCGCGCGTAATCCGGCG	1	54
-5974	ATCCGGATGAAGCCGCTT	GCAATGTATGTCGTTTCA	1	21
-6666÷4	GCCGTAAGTCTTGATCTC CTTA	CCTCATCAGTGGCTCTAT	1	22
-7430	TTTGAATGGTTCGCGGCG	CGTAGCGGTGGAAGTGGC	1	21
-9265	TTGTGCCACGCATCATCC	ATGGATGCAGCCTCCAGA	1	21
1.5				
-3219	GTAATAGCGATGCGTAAT	AGGAAAACAGGAAAGGGG	1	61
-7081	TCAGCCAGCTTCCCAGCC	GGTGGAAGTGGCGATGAA	1	30